Process Modelling and Optimization of Methanol-to-Jet for eSAF

Aleyna Sandzhakla

Hydrogen Technology and Fuel Cell Systems, HYTEC4-1013, 2025-05

4th M.Sc. Semester Master Thesis

AAU Energy
Aalborg University
http://www.aau.dk

AALBORG UNIVERSITY
STUDENT REPORT

Title:
Process Modelling and Optimization of Methanol-to-Jet for eSAF

Theme:
eSAF synthesis

Project Period:
Spring Semester 2025

Project Group:
HYTEC4-1013

Participants:
Aleyna Sandzhakla

Supervisors:
Daniele Castello
Xiaoti Cui

Number of Pages: 64

Date of Completion:
May 28th - 2025

Abstract:

To reach long-term greenhouse gas (GHG) neutrality in aviation, replacing fossil-based jet fuels with Sustainable Aviation Fuels (SAF) from renewable sources is crucial. This study investigates the process modeling and optimization of the Methanol-to-Jet (MtJ) pathway for e-SAF production using Aspen Plus V12.1, integrating methanol synthesis from CO_2 and H_2, methanol-to-olefins (MTO) conversion, oligomerization, and hydrogenation. A novel dynamic modeling approach was implemented for oligomerization, linking a custom MATLAB model to Aspen Plus via Excel to predict product distribution using the Anderson–Schulz–Flory (ASF) mechanism parameterized by reactor conditions. Process optimization through response surface methodology targeted maximization of kerosene yield and minimization of cost. The optimized process achieved a kerosene yield of 0.40 Cmole/Cmole, a sustainable aviation fuel production rate of 9395 tonnes/year, and a Levelized Cost of SAF (LCOSAF) of 6980 €/tonne. Overall, the results demonstrate the technical feasibility and optimization potential of the MtJ process, but further reductions in feedstock cost and improved heat integration are needed for economic viability at scale.

Summary

This thesis presents a comprehensive process modeling and optimization study of the Methanol-to-Jet (MtJ) pathway for the production of sustainable aviation fuel (e-SAF) from renewable hydrogen and captured CO_2. The increasing urgency to decarbonize aviation has accelerated research into Power-to-Liquid (PtL) pathways, with MtJ emerging as a promising alternative, particularly due to its flexibility and compatibility with renewable energy inputs. This work employs Aspen Plus V12.1 for steady-state process simulation, systematically incorporating key process steps: methanol synthesis from CO_2 and H_2, methanol-to-olefins (MTO) conversion, oligomerization, and hydrogenation, with all major separation and compression units included.

A distinctive feature of this project is the integration of a custom MATLAB model for the oligomerization reactor, dynamically connected to Aspen Plus via Excel. The oligomerization model is based on the Anderson–Schulz–Flory (ASF) product distribution, where the chain growth probability parameter (α) is parameterized as a function of temperature and pressure. This approach enables the prediction of hydrocarbon product distributions under varying conditions, aligning the simulation output with experimental trends from literature. Model calibration and validation were performed using experimental data, achieving a good degree of accuracy across a range of operational scenarios. The simulation was used to investigate and optimize the key operating variables, applying response surface methodology (RSM) to balance kerosene yield against overall process cost. The main optimization variables included methanol reactor pressure and oligomerization reactor temperature and pressure. Multi-objective optimization identified process conditions that maximize jet fuel output while reducing the total capital cost.

A techno-economic assessment was also conducted to evaluate the cost structure and identify the main economic drivers for MtJ-based eSAF. Under optimized conditions, the process achieved a kerosene yield of 0.40 Cmole/Cmole and an annual e-SAF production rate of 9395 tonnes, with a Levelized Cost of SAF (LCOSAF) of 6980 €/tonne. The cost analysis results showed that feedstock prices, especially for green methanol, constitute the largest share of the LCOSAF. It is important to note that heat integration was also not implemented in this study, and all utility requirements were met with external heating and cooling. These findings highlight the necessity for further cost reductions in renewable hydrogen and CO_2 supplies to ensure economic viability, as well as the potential for future process improvements through energy integration.

The study also mentioned the technical flexibility of the MtJ process. The modeling structure allows for the adjustment of key parameters, enables robust process optimization and supports its implementation at both pilot and commercial scales. The process can produce e-SAF that meets ASTM D7566 quality standards in terms of boiling points, even though MtJ is not yet approved under ASTM certification. Additionally, the process can generate valuable by-products such as naphtha and light hydrocarbons, which can

be recycled or sold to improve the overall process economics. While this work focused on kerosene as the target product, future studies might consider a more comprehensive utilization of by-products and investigate advanced energy and process integration strategies.

From a larger perspective, the findings underline the significant potential of MtJ as a scalable and flexible pathway for sustainable jet fuel production. However, the realization of economic competitiveness depends on continued progress in renewable feedstock supply chains, technology improvements, and effective policy support for synthetic fuels.

In conclusion, this thesis provides a detailed assessment of the MtJ process for e-SAF, integrating advanced modeling and optimization tools to demonstrate its feasibility and potential for further improvement. The link between process modeling and economic evaluation supports decision-making for both industry and policymakers. While current cost barriers remain, the MtJ route offers a credible and adaptable solution for aviation decarbonization, justifying further research and development in both technical and economic dimensions.

Preface

This Master thesis has been written by 4th semester M.Sc. student, HYTEC-1013, at the Department of Energy of Aalborg University. Regarding this thesis, I want to acknowledge my supervisors Daniele Castello and Xiaoti Cui from the Aalborg University.

Reading Guide

The citations have been done using the Harvard referencing method where citations. The citations follow their references in the bibliography located at the end of the thesis. Chapters, sections, figures, tables and equations are labeled and these will also be references when mentioned in the text. The numbering of these labels is in chronological order and chapter-wise. Figures, calculations and additional theory not included in the report will be found in the Appendix.
The following software has been used in this project:

- Aspen Plus
- Mathworks MATLAB
- Microsoft Excel
- Overleaf Latex

Aleyna Sandzhakla Signature: 

Nomenclature

Symbol	Explanation	Unit
A	Cash flow	€
C	Cost	€
E	Activation energy	kcal/mol
Gp	Gross profit	€
H	Enthalpy	kJ/mol
K	Adsorption equilibrium constant	1/bar
K	Adsorption term or equilibrium constant	-
P	Annual production rate	ton/year
P	Pressure	Pa, bar, or barg
R^2	R squared value	-
S	Selectivity	-
T	Temperature	°C or K
W	Weight	-
X	Conversion	-
Y	Yield	-
c_o	Cost of manufacturing	€
d	Depreciation	€
f	Inflation rate	-
i	Discount rate	-
k	Rate constant	mol/kg/s
k	Number of factors in Central composite design	-
n	Number of years	year
$\dot{n}$	Molar flow rate	kmol/hr
N_p	Net Profit	€
r	Reaction rate	mol/kg/s
s	Sales revenue	€
x, y, z	Power law exponents	-

Greek symbols

Symbol	Explanation	Unit
α	Chain Growth Probability	-
α	Distance factor of the axial (or star) points	-
β	Response surface coefficient	-
η	Efficiency	-
ρ	Density	mol/m^3
θ	Income tax rate	-

Subscripts

Subscript	Explanation
A	First adsorption term
B	Second adsorption term
C	third adsorption term
D	Fourth adsorption term
O	Olefin subscript
n	Carbon number
DME	Dimethyl ether synthesis reaction
EtOH	Ethanol synthesis reaction
MS	Methanol synthesis reaction
RWGS	Reverse water-gas shift reaction
ref	Reference value

Unit labels in process flow diagrams

Unit label letter	Unit
C	Distillation column
E	Heat exchanger
K	Compressor
R	Reactor
V	Vessel

Abbreviations

Abbreviation	Explanation
ASF	Anderson-Schultz-Flory
ASTM	American Society for Testing and Materials
ATJ	Alcohol-to-jet
BtL	Biomass-to-liquid
CAPEX	Capital Expenditures
CCD	Central composite design
CEPCI	Chemical Engineering Plant Cost Index
CORSIA	Carbon Offsetting and Reduction Scheme for International Aviation
DAC	Direct air capture
DDE	Dynamic data exchange
eSAF	Sustainable Aviation Fuel
EU	European Union
FT	Fischer-Tropsch
GHG	Greenhouse Gas
HYDRO	Hydrogenation
IEA	International Energy Agency
KERCOL	Kerosene distillation column
LCOP	Levelized Cost of Production
LCOSAF	Levelized Cost of Sustainable Aviation Fuel
LHHW	Langmuir-Hinshelwood-Hougen-Watson
MSE	Mean squared error
MtJ	Methanol-to-Jet
MtO	Methanol-to-olefins
NPV	Net Present Value
NTRTL-RK	Non-Random Two-Liquid activity coefficient model for the liquid phase with the Redlich-Kwong equation of state for the vapor phase
OPEX	Operating Expenditures
OLI	Oligomerization
PBR	Packed Bed Reactor
PE	Purchased Equipment
PEM	Proton exchange membrane
PR-BM	Peng–Robinson-Boston–Mathias
PtL	Power-to-liquid
PtX	Power-to-X
PWF	Present Worth Factor

Abbreviation	Explanation
REGEN	Regenerator
RED	Renewable Energy Directive
RFNBOs	Renewable fuels of non-biological origin
RKSMHV2	Redlich-Kwong-Soave EOS with the Modified Huron-Vidal mixing rule
RSM	Response surface methodology
RWGS	Reverse Water Gas Shift
SAF	Sustainable Aviation Fuel
SOEC	Solid oxide electrolyzer cell
SPK	Synthetic Paraffinic Kerosene
SSE	Sum of squared error
VLE	Vapor-Liquid-Equilibrium

Contents

Chapter 1

Introduction

1.1 Background and Motivation

The Paris Agreement, which was signed by 196 countries in 2015, aims to limit global warming to 2°C above pre-industrial levels by reducing greenhouse gas (GHG) emissions and achieving net-zero emission targets. This requires major changes in the energy and industrial sectors. The aviation sector is one of the significant contributors to global carbon dioxide (CO_2) emissions, contributing to approximately 2-3 % of global energy-related CO_2 emissions, reported in 2023 [International Energy Agency, 2025].

On the international level, the International Civil Aviation Organization (ICAO), a United Nations agency, introduced a "basket of measures" that includes improvements in aircraft technologies in response to the Paris Agreement, including aircraft technology, operational improvements, sustainable aviation fuels, and the Carbon Offsetting and Reduction Scheme for International Aviation (CORSIA). Under CORSIA, countries are required to offset aviation-related emissions from 2027 to 2035 to maintain their 2020 levels [UNFCCC, 2018].

The European Union (EU) is among the most proactive regions employing strong policy support in favor of sustainable aviation fuel (SAF) for decarbonizing the sector. The ReFuelEU Aviation initiative requires the use of SAF for all flights departing from the EU. The regulation sets a minimum SAF blending target of 2 % in 2025 and reaching 70 % by 2050. In addition, a sub-mandate for synthetic aviation fuels (e-SAF) is introduced, requiring 1.2 % by 2030 and 35 % by 2050 [Larsen et al., 2023]. Additionally, the Renewable Energy Directive (RED III) supports SAF deployment by applying a 1.5x multiplier for renewable fuels of non-biological origin (RFNBOs) used in aviation [Chirita, 2024]. EU mandates will require over 2 million tons of SAF by 2030, while current projections indicate that only about 10 % of this demand will be met through available production facilities [Larsen et al., 2023]. All of these are encouraging the usage and development of SAF, especially e-SAF.

In addition to EU-level policies, the Danish government is also taking steps to support SAF deployment. Denmark's national Power-to-X (PtX) strategy targets the installation of 4–6 GW of electrolysis capacity by the year 2030, which can unlock pathways for green hydrogen, e-SAF, and other renewable fuel pathways. As of March 2024, Danish PtX project announcements total up to 17.8 GW of expected capacity, from which approximately 1.2 GW is expected to supply the aviation sector, enabling the production of an estimated 236,000 tonnes of e-SAF annually [Clarkfeldt and Kristensen, 2024].

Several significant e-SAF projects have been announced in Denmark in recent years, reflecting strong industry commitment and policy support for green aviation fuels. Fjord PtX project which is located in Aalborg is designed to deploy industrial-scale electrolysis technology, at the megawatt level, to produce e-SAF. [CIP, 2025]. Another major Danish initiative is led by European Energy, which is advancing Power-to-X projects in Southern Denmark. Their Power-to-X projects include green hydrogen, e-methanol and e-SAF for use in both aviation and shipping, illustrating the integration of PtX solutions across multiple sectors [Energy, 2025]. These projects exemplify Denmark's role in scaling up PtX-based SAF production, with direct contributions to both national decarbonization goals and the EU's targets for renewable fuels in aviation.

1.1.1 Alternatives Towards Decarbonization of Aviation Industry and Sustainable Aviation Fuel

In the way of decarbonizing the transportation sector, sustainable alternatives started to emerge. Figure 1.1 shows different pathways for sustainable transportation, including electric vehicles (hybrid or fully electric), non-drop-in fuels (such as hydrogen, methanol, etc.), which cannot be directly used in existing infrastructure or engines, and drop-in fuels (such as SAF, diesel, gasoline, etc.), which enable direct substitution into built-in engines of infrastructure. In addition to fuel production, it is also possible to produce byproducts such as methanol and naphtha to use as feedstock in chemical production processes.

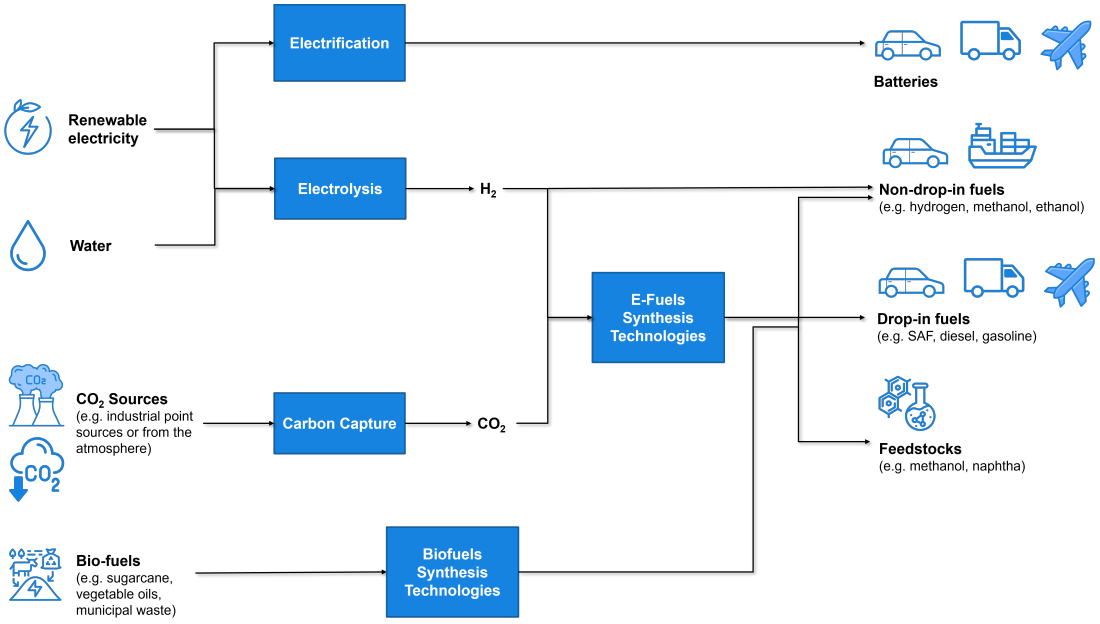

Figure 1.1: Sustainable solutions for decarbonizing transportation sector.

Electrification is very popular among relatively lightweight vehicles and has been improving itself for the last few years. However, electrifying aircraft is challenging in terms of energy storage limitations, especially for long-distance applications. Hydrogen is a viable long-term sustainable fuel, but it demands substantial changes to the existing fuel infrastructure and machinery. Biofuels, produced from biomass (BtL), have attracted attention for their environmental benefits compared to fossil fuels. In jet fuel concept, Hydroprocessed Esters and Fatty Acids (HEFA) is one of the first commercially advanced BtL pathways, which converts vegetable oils, animal fats, or waste oils into jet fuel through catalytic hydrogenation. Another BtL route is thermochemical gasification. In this process, solid biomass is converted into syngas (a mix of CO and H), which is then catalytically processed into SAF via Fischer-Tropsh (FT), or via a methanol intermediate and methanol-to-jet (MtJ) conversion. In addition to that, syngas fermentation may also be possible which can subsequently be used for alcohol-to-jet (AtJ) process. AtJ is a biochemical pathway in which alcohols such as ethanol or isobutanol, derived from biomass, are converted into jet-range hydrocarbons. However, the sustainability of biomass-based fuels is dependent on the source of biomass. Another critical challenge in BtL processes is the inherently low energy density of raw biomass, which increases transportation and handling costs. And lastly, they are also constrained by the finite availability of biomass resources. In contrast, products of Power-to-Liquid (PtL) processes, so-called e-fuels, which utilize carbon dioxide from the atmosphere, hold the potential for large-scale implementation without the limitations of limited biomass feedstocks. PtL technologies, although less developed than BtL processes, have advantages such as high energy density and the ability to enable sector coupling. [IEA Bioenergy Task 39, 2023, Bube et al., 2025, Eyberg et al., 2024]

The Power-to-Liquid (PtL) pathway does not require any biomass feedstocks in theory, since a mixture of CO_2 from carbon capture and H_2 from electrolysis serves as the feed gas for the subsequent step of liquid product formation, which is fuel in this case. In renewable jet fuel production, H_2 can be generated via low-temperature electrolysis methods, such as Alkaline and Proton Exchange Membrane (PEM) electrolyzers, or through high-temperature electrolysis using Solid Oxide Electrolyzer Cells (SOECs). The choice of electrolyzer depends on factors such as operating temperature, cost, and technology readiness level. For instance, while low-temperature electrolyzers are commercially available and widely used, SOECs have recently attracted attention due to their higher efficiency, despite being more expensive than their counterparts. CO_2 can be captured from point sources like conventional power plants, from air via Direct Air Capture (DAC) technologies, or from biogenic production. [Larsen et al., 2023]

The source of CO_2 (either from the air or industrial sites) and the fuel synthesis method determine how electricity, air, water, or biomass turn into e-kerosene. Especially if alkaline electrolyzers are used, the low quality heat (at temperature of 50-60 °C) can be repurposed for district heating. This utilization of waste heat can provide an additional

revenue stream, improving the economic viability of e-jet fuel and earning points against fossil-based alternatives. There are two main eSAF pathways:

1. **e-SAF production via Fischer Tropsch (FT) synthesis** – This pathway uses syngas (CO and H_2) to generate synthetic crude, often referred to as e-crude which is then refined into jet fuel. In order to convert CO_2 into CO, a reverse water gas shift (RWGS) reactor is utilized, which requires a significant amount of heat and operates at very high temperatures. On the other hand, FT synthesis reaction is exothermic, which is beneficial for energy recovery. There are two different process types, which are Low-Temperature Fischer–Tropsch (LTFT) operating at 180-250 °C, and High-Temperature FT (HTFT) operating at 300-375 °C. Low-Temperature Fischer–Tropsch (LTFT) is generally preferred for jet fuel production due to its higher selectivity toward long-chain hydrocarbons in the jet fuel range (C8–C16). It produces waxes that can be easily upgraded to jet fuel via hydrocracking, making it more suitable than High-Temperature FT (HTFT), which favors lighter products. FFT-SPK (Fischer–Tropsch Synthetic Paraffinic Kerosene) is also ASTM-certified and can be blended with conventional jet fuel at ratios of up to 50 %. [Larsen et al., 2023, Maitlis and de Klerk, 2013]

2. **e-SAF production via Methanol-to-Jet process** – This pathway also uses CO_2 and H_2 to synthesize methanol (MeOH) first, either with or without converting CO_2 to CO. Methanol synthesis is also exothermic as FT reaction, whose heat can be integrated into H_2 production, or CO_2 capture, for instance. Green MeOH is then converted to SAF through a combined Methanol-to-Olefins (MTO) and olefin oligomerization process. In the MTO step, short olefins such as ethylene and propylene are synthesized from MeOH. These olefins are subsequently oligomerized to form longer hydrocarbons, which are then hydrogenated to produce e-crude. This e-crude can be further refined into jet fuel-range hydrocarbons. While the FT pathway is already ASTM-approved for SAF production, the MtJ pathway is yet to be certified [IEA Bioenergy Task 39, 2023, Larsen et al., 2023].

Despite its promise in decarbonizing aviation, the PtX route for e-SAF production still have some limitations. PtX is highly energy-intensive, as it relies on renewable electricity for water electrolysis and CO_2 conversion, which leads to scalability and cost challenges due to limited availability of low-cost renewable energy. The overall efficiency of the process is also relatively low, given the multiple energy conversion steps involved, leading to significant energy losses [Schmidt and Weindorf, 2018]. Economically, PtX-based eSAF remains considerably more expensive than conventional jet fuel, primarily due to high capital expenditures for electrolyzers and synthesis units, as well as the operational costs tied to fluctuating electricity prices [Vickers et al., 2020]. In this context, in addition to the importance of strong policy support as discussed, ensuring the economic feasibility of the eSAF pathway is equally important to enable its real-world implementation.

1.1.2 Jet Fuel Specifications

ASTM D1655, "*Standard Specification for Aviation Turbine Fuels*," is one of the most well-known fuel quality standards that the international aviation industry complies with. In response to the introduction of alternative fuels, ASTM developed D7566, "*Standard Specification for Aviation Turbine Fuel Containing Synthesized Hydrocarbons*", which establishes stricter requirements for synthetic fuels lacking operational history. D7566 allows certified synthetic fuels to be integrated into the current fuel infrastructure by allowing them to be reclassified as D1655 fuels, which is for conventional jet fuels, after being blended. For Fischer–Tropsch Synthetic Paraffinic Kerosene (FT-SPK), which primarily consists of paraffins and lacks sufficient aromatic content, blending is typically 8–20 % by Jet A-1 standards. As a result, these fuels must be blended with conventional kerosene to meet density and aromatic requirements. Even for variants such as FT-SPK/A, which include aromatic components and shows a very similar composition to conventional jet fuel, a 50 % blending is imposed [Rumizen, 2021]. Alcohol-to-Jet Synthetic Paraffinic Kerosene (ATJ), which is derived from ethanol and isobutanol and primarily consists of isoparaffins, is also certified under ASTM D7566. At present, a maximum blending ratio of 50% is allowed to ensure compliance with the standards. However, MtJ is not yet covered under this certification and is still undergoing the approval process. [Rumizen, 2021, IEA Bioenergy Task 39, 2023].

According to ASTM D7566 specifications, the physical distillation characteristics of jet fuel should meet the following requirements: the temperature at which 10% is recovered (T10) must not exceed 205 °C, and the final boiling point must not exceed 300 °C [ASTM International, 2012]. Additionally, two key properties are its low freezing point, which must be below −47 °C, and viscosity, which should not exceed 8 mm^2/s at −20 °C, and typically falls within the range of 1–2.5 mm^2/s at 38 °C. These qualities ensure that the fuel remains fluid and operational at the low ambient temperatures encountered during high-altitude flights [Shell, 2024].

1.1.3 Methanol-to-Jet Fuel (MtJ) Pathway

The goal of this study is to simulate MtJ PtL pathway for SAF production from hydrogen (H_2) obtained from the electrolyzer and carbon dioxide (CO_2) from carbon capture using Aspen Plus V12.1. The MtJ pathway consists of methanol synthesis, methanol-to-olefin conversion, oligomerization, hydrogenation and refining as seen in Figure 1.2.

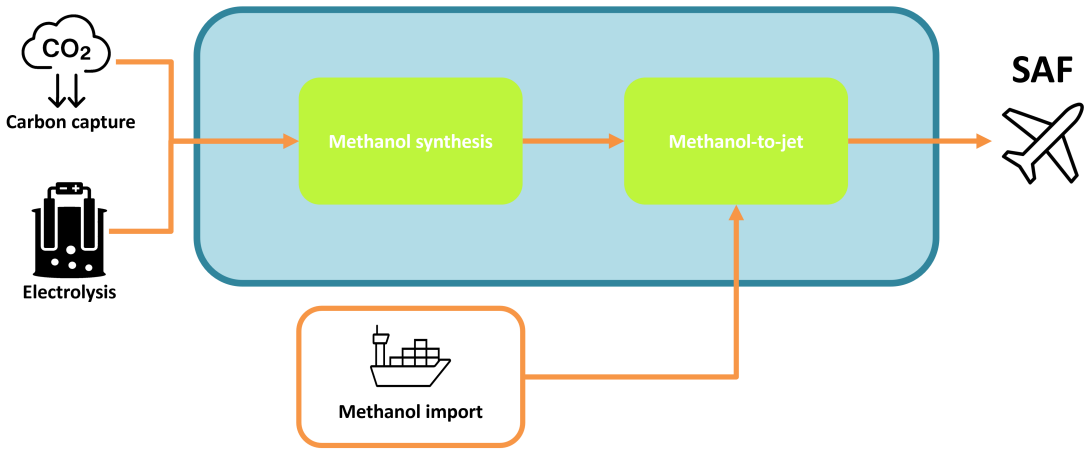

Figure 1.2: Methanol-to-jet pathway.

Methanol synthesis from CO_2 and H_2 produces a mixture of methanol and water, which is then separated via distillation. The conversion of methanol into hydrocarbons was primarily developed during the 1970s, with the Mobil Olefins to Gasoline and Distillate (MOGD) process being one of the key technologies commercialized in the 1980s [Börner, 2014]. However, these efforts were mainly focused on producing shorter-chain hydrocarbons, such as gasoline, rather than kerosene [Bube et al., 2024]. Similar to other alcohol-based fuel pathways, such as Alcohol-to-Jet (AtJ), MtJ conversion involves olefin formation through dehydration, followed by oligomerization into longer-chain olefins. A following hydrogenation step saturates these olefins to paraffins, and the final fuel fractions are obtained through distillation [Bube et al., 2024].

1.1.4 The Importance of Process Modelling

Shifting towards sustainable aviation fuels is essential to meet both EU and global climate goals and to reduce the aviation sector's carbon footprint. The development and optimization of Power-to-Liquid (PtL) pathways, particularly the Methanol-to-Jet (MtJ) process, represent a significant step toward achieving these objectives. However, experimental validation of such complex processes at full scale is often impractical due to the high number of interconnected units, the system's technical complexity, and the considerable financial resources required. Process modeling thus provides a crucial tool for early-stage evaluation of performance and profitability before any real investment is made. It enables systematic analysis of process parameters, supports optimization of operating conditions, and helps in design decision-making process and lower the risk in investment before physical implementation.

1.2 State of the Art

The increasing urgency to decarbonize aviation has accelerated the development of sustainable aviation fuels (SAFs), particularly those based on renewable electricity and carbon dioxide via power-to-liquid (PtL) routes. Among the most promising pathways, the Fischer–Tropsch (FT) synthesis and Methanol-to-Jet (MtJ) process have received considerable attention for their potential to replace fossil jet fuels while leveraging existing infrastructure [Bube et al., 2024, Eyberg et al., 2024].

Methanol, which can be synthesized from syngas or directly via CO_2 hydrogenation, serves as a flexible intermediate for further conversion to hydrocarbons. Green methanol synthesis technologies are well established, often modeled using the Vanden Bussche and Froment kinetics for $Cu/ZnO/Al_2O_3$ catalysts [Bussche and Froment, 1996]. This reaction network, coupled with commercial process simulators like Aspen Plus, enables accurate reactor design and process optimization [Aspen Technology, Inc., 2021]. CO_2-based methanol production has also been validated through simulation and energy integration studies, supporting its role in future SAF scenarios [Vandal and Bouallou, 2013].

The downstream conversion of methanol to jet-range hydrocarbons typically involves dehydration (MTO), oligomerization (OLI), and hydrogenation (HYDRO) steps. The MtJ process largely evolved from the Mobil Olefins to Gasoline and Distillate (MOGD) technology. Originally designed to convert methanol into gasoline and diesel-range products, MOGD employed a combination of MTO, OLI, and HYDRO steps. Current MtJ processes take inspiration from the original MOGD setup, adjusting the reaction conditions and catalysts to focus on making jet fuel-range hydrocarbons instead of gasoline. This connection to a well-established technology gives MtJ a solid foundation. In MOGD process, both for MTO and oligomerization, ZSM-5 catalyst typically has been used. MTO catalyst can be divided into two major groups: "small pore" such as ZSM-34 and SAPO-34, and "medium pore" such as ZSM-5. The small pore catalysts generally yield C4 products while the medium pore ones typically yield higher chain hydrocarbons (C5+). Additionally, small pore catalyst are sensitive to coke formation more. [Avidan, 1988]

Early MTO processes, such as the MTG (Methanol-to-Gasoline) and MOGD routes developed by Mobil, relied on ZSM-5 zeolites mostly, which favor aromatic-rich gasoline. Later innovations introduced SAPO-34 catalysts, which enabled higher selectivity toward light olefins. In terms of reactor design, both fixed-bed and fluidized-bed systems have been applied in MTO implementations. Union Carbide was a key factor for the upscaling of MTO process due to the high selectivity of light olefins, which utilizes SAPO-34. SAPO-34 is highly stable, combining a regeneration reactor for coke combustion. Among the key industrial advancements, the MTO technology developed by UOP/Norsk Hydro played a pioneering role, beginning with the installation of a pilot plant in Nor-

way in 1995. Since then, industrial-scale MTO has expanded globally, with four prominent technologies gaining traction, particularly in China: (i) DMTO by the Dalian Institute, (ii) S-MTO by Shanghai Research Institute of Petrochemical Technology (SRIPT) and Sinopec, (iii) MTP (methanol-to-propylene) by UOP/Norsk Hydro, and (iv) MTP by Lurgi. [Cordero-Lanzac et al., 2024] These advances allowed continuous operation and scalable production and commercialization of MTO technologies which creates the groundwork for advancements in MtJ process.

In terms of modelling, MTO has been modelled using a kinetic reactor (RPLUG in Aspen) with kinetic data, a yield reactor (RYIELD in Aspen) and a fixed conversion reactor (RSTOIC in Aspen). In terms of kinetic models, several different models have been established to capture the complex reactions behavior in MTO processes. These models are generally divided into two categories: lump models, and detailed models considering individual reaction steps. Aguayo et al. developed a seven-lump kinetic model for methanol conversion over HZSM-5 in a fixed-bed reactor, operating under isothermal conditions. Similarly, Kaarsholm et al. also developed a lump kinetic model for the MTO reaction using a phosphorus-modified ZSM-5 catalyst in a small-scale fluidized-bed reactor, employing a two-phase (bubble and emulsion) model, again under isothermal conditions [Kaarsholm et al., 2010].

In the PhD thesis of Wahabi et al., a detailed kinetic model based on elementary steps for the MTO process on SAPO-34 was developed [Al Wahabi, 2003]. Several reactor modes were also investigated based on the developed kinetics, including isothermal and adiabatic in both packed-bed and fluidized-bed reactors. Subsequently, Wahabi and Froment developed a fundamental single-event kinetic model for the MTO process over SAPO-34, using a detailed reaction network with over 700 elementary steps [Al Wahabi and Froment, 2004]. A study by Najafabadi et al. proposed a kinetic model for methanol conversion over SAPO-34, emphasizing lumped kinetic modeling to evaluate operating parameters like temperature, pressure, and water/methanol ratio [Taheri Najafabadi et al., 2012]. The model used a genetic algorithm for parameter optimization and highlighted ethylene and propylene yield improvements under varied space–time conditions. Yu and Chien provided a steady-state simulation framework for MTO process [Yu and Chien, 2016]. In their study, MTO fluidized-bed reactor was modeled as an isothermal RPLUG reactor for simplicity, including a lumped kinetic expression from Ying et al. [Ying et al., 2015]. Chang et al. developed a 3D CFD model for a fluidized-bed MTO reactor, coupling a lumped kinetic model for SAPO-34 catalyst with a two-fluid flow hydrodynamic model [Chang et al., 2013]. The kinetic model was adapted from Chen et al., which also accounted for the catalyst deactivation [Chen et al., 2007]. For design purposes, lumped kinetics are used in most cases due to the fact that the detailed models are often time-consuming and impractical [Chang et al., 2013].

While kinetic models provide a deeper understanding of the reaction mechanism, simplified approaches like the RYIELD reactor are often preferred in process simulations to estimate product distributions quickly and efficiently. Salkuyeh and Adams developed a polygeneration process that produces olefins, MeOH, DME, and electricity from conventional pipeline natural gas and different kinds of shale gases. They modeled the MTO section using an RYield reactor block in Aspen Plus, simulating the UOP/Hydro MTO process, with SAPO-34 as the catalyst [Salkuyeh and Adams, 2015]. The model emphasized selectivity outcomes based on experimental data by Wilson et al. rather than detailed reaction kinetics [Wilson and Barger, 1999]. Ortiz-Espinoza et al. modeled the MTO process as a part of a larger shale gas-to-ethylene conversion pathway, using an RYield reactor block in Aspen Plus [Ortiz-Espinoza et al., 2017]. The model employed a SAPO-34 catalyst and used experimental product distributions from Vora et al. to estimate yields [Vora et al., 1997].

Unlike the MTO process, the MOGD section, which includes oligomerization, hydrogenation, and hydroisomerization (optional), lacks sufficient literature work in kinetic modelling. Although early studies such as Alberty's assumed uniform reaction rates across olefin species and equilibrium-controlled reversibility [Alberty, 1987], more recent research by Dubray et al. has demonstrated that reaction rates differ significantly between molecules [Dubray et al., 2022]. In addition to that, ZSM-5 which is also commonly used in MOGD process, is a shape-selective zeolite catalyst; its pore size and structure only allow certain-sized molecules to enter and react. This means long-chain molecule formations would be hindered, and at full conversion, product distribution was found to be largely independent of the carbon number of the feedstock olefin [Tabak et al., 1986]. Dubray et al. and Garwood's studies also support that the product distribution is independent of the carbon number of the olefin feed [Dubray et al., 2022, Garwood, 1983]. On the other hand, there is also an approach that relies on a statistical framework for modeling the product distribution from olefin oligomerization which propose the dependence of distribution with the yield carbon number. Two statistical models are proposed: Poisson and Anderson–Schulz–Flory (ASF) distributions [Nicholas, 2017]. Poisson distribution applies when chain growth is random and each step has an equal probability of termination, regardless of chain length. This only happens in highly controlled systems, such as some metal-catalyzed reactions, and is not common in real fuel production. ASF distribution, on the other hand, is more realistic for most fuel-related processes. It assumes that after each propagation step, the chain has a fixed probability to keep growing, which fits well with the behavior of acid catalysts like ZSM-5, which is commonly used in MtJ process. These catalysts often allow olefins to rejoin the reaction and form longer chains. In Bube et al.'s model, oligomerization is also assumed to follow an ASF distribution, similar to FT synthesis, and accounts for the feed carbon number when defining the product distribution [Bube et al., 2024]. Given that, detailed kinetics are not able to reliably capture the full complexity of the oligomerization mechanisms, hence, simplified or empirical values

for product distribution are often used in modeling.

Several recent techno-economic assessment studies evaluate process efficiency, carbon utilization, and cost performance between MtJ and FT pathways, demonstrating that MtJ may offer superior energy efficiency and flexibility under certain conditions. Ruokonen et al.'s work is on the MTO-MOGD process simulation with Aspen Plus, modeling a pilot-scale production of gasoline, kerosene, and diesel from renewable methanol [Ruokonen et al., 2021]. The MTO reactor was selected as an isothermal reactor with full conversion of methanol to DME and light olefins over ZSM-5 catalyst. The MOGD reactor oligomerized olefins, again using ZSM-5 in isothermal mode, followed by hydrogenation and hydroisomerization steps. Experimental yields for oligomerization were obtained from Avidan [Avidan, 1988]. Additionally, they performed a techno-economic analysis estimating the total product cost (TPC) is 3409 €/ton of fuel, corresponding to a renewable MeOH price of 963 €/ton of MeOH. Compared to the present price of fossil fuels and biofuel blending components, the estimated fuel price is significantly higher, indicating that significant improvements in MeOH sourcing, which comes from electrolytic hydrogen, or financial incentives would be necessary for economic competitiveness under current market conditions. The analysis also revealed that methanol feedstock cost accounts for approximately 70 % of operational expenses, making it the most critical factor affecting overall production costs.

Vincent Eyberg et al. carried out process simulations with nine configurations and followingly, a techno-economic assessment of two Power-to-Liquid (PtL) pathways, Fischer–Tropsch (FT) and Methanol-to-Jet (MtJ) approaches, with CO_2 sourcing from direct air capture (DAC) and H_2 sourcing from solid electrolyzers (SOEC) [Eyberg et al., 2024]. In their Aspen Plus simulation, kinetic models of Mignard et al. and Aguayo et al., respectively for MeOH synthesis and MTO process [Mignard and Pritchard, 2008] [Aguayo et al., 2010]. The oligomerization section was inspired by MOGD process, using a model derived from an empirically determined product distribution by Avidan [Avidan, 1988]. Their study found that, although MtJ processes required larger electrolyzers and had slightly higher fuel production costs compared to Fischer–Tropsch, both pathways achieved similar syncrude Levelized Cost of Production (LCOP) values around 0.81 €/kWh for 2022 conditions. Future projections showed significant cost reduction potentials with advancements in DAC and SOEC technologies by 2050.

In the Bube et al.'s study, both FT and MtJ pathways for kerosene production were simulated using Aspen Plus [Bube et al., 2024]. It was assumed there was no internal heat integration initially; instead, a pinch analysis was later performed separately using Aspen Energy Analyzer to estimate the minimum external heating and cooling demands. Although the model did not include a comprehensive heat exchanger network, the pinch

analysis allowed them to assess the potential for energy savings. Different parameter variations, such as chain growth probability and hydrocracking behavior in FT and dehydration olefin selectivity and oligomerization product distribution in MtJ, were explored to evaluate the effects on carbon and energy efficiency and to indicate uncertainties and optimize the kerosene production. Using the simulations from this work, Bube et al. also performed a techno-economic assessment to compare the two pathways [Bube et al., 2025]. For the cost analysis, two allocation strategies were defined: kerosene allocation which excludesby-product revenues, and total fuel allocation which includes by-product revenues such as naphtha and diesel. Economically, for total fuel allocation, FT yields less total product cost (TPC) while for kerosene allocation MeOH yields less. In all cases, costs are mainly influenced by H_2 and CO_2 supply and conversion efficiency of them.

In summary, methanol-based SAF synthesis shows a great potential to replace the fossil jet fuel. However, successful deployment depends on continued advancements in process integration, catalyst development, regulatory approval, and the scale-up of renewable electricity and carbon capture infrastructure. This work aims to build upon previous studies by developing a comprehensive MtJ process simulation and performing an updated techno-economic evaluation under current and projected energy market conditions.

Considering the literature, studies often apply fixed distribution model from experimental data for the oligomerization process, this work includes a versatile product distribution model which enables observing the change in product distribution with different pressure and temperature. By doing so, the process can be realistically optimized and assessed for techno-economic viability.

Chapter 2

Objective

The aviation industry needs to switch from fossil fuels to Sustainable Aviation Fuels (SAF), which are produced from renewable energy sources, in order to neutralize greenhouse gas (GHG) emissions in the long term. Methanol-to-Jet (MtJ) pathway is one of the most interesting SAF options among Power-to-Liquid (PtL) processes. However, the MtJ pathway also faces several challenges, including relatively high production costs due to the current price of renewable methanol which is produced from green hydrogen and captured CO_2, the need for further catalyst development, and the lack of ASTM certification for commercial jet fuel applications. In this sense, this thesis focuses on:

Designing and evaluating a sustainable Methanol-to-Jet (MtJ) fuel production process using Aspen Plus including key process units such as methanol synthesis, methanol-to-olefins (MTO), oligomerization, and hydrogenation, to achieve jet fuel production from CO_2 and hydrogen feedstock. The study aims to optimize operational conditions in favor of increasing kerosene yield and reducing overall expenses through process modeling, as full-scale experimental testing is impractical due to the system's complexity and the significant costs involved.

2.1 Approach

The problem statement will be investigated through the following steps:

1. **Process Design:** Develop a complete process model in Aspen Plus, including the methanol synthesis from CO_2 and H_2, MTO conversion, olefin oligomerization, and hydrogenation to produce jet fuel-range hydrocarbons.
2. **Simulation and Optimization:** Perform steady-state simulations at different selected operating conditions which are pressure of methanol reactor, temperature and pressure of oligomerization reactor to determine kerosene yield, compositions, and costing. Optimize those process conditions to maximize jet fuel production with a trade off of capital cost.
3. **Techno-Economic Analysis:** Evaluate the Levelized Cost of eSAF (LCOSAF) and identify key cost drivers and performance bottlenecks.

Chapter 3

Process Description and Simulation Approach

3.1 Aspen Plus Model Setup, Assumptions and Limitations

Throughout the process, the simulation approach is mainly based on the PR-BM (Peng – Robinson - Boston – Mathias) method. For the methanol synthesis section, RKSMHV2 (Redlich-Kwong-Soave EOS with the Modified Huron-Vidal mixing rule) for pressures above 10 bar since it is appropriate for high pressure and high temperature conditions, and systems involving non-polar and polar compounds. For pressures below that threshold, NTRTL-RK (Non-Random Two-Liquid activity coefficient model for the liquid phase with the Redlich-Kwong (RK) equation of state for the vapor phase) method is selected. [Eyberg et al., 2024]

The commercial software Aspen Plus V12.1 was used for process design and simulation. According to literature, centrifugal compressors can handle discharge temperature up to 200-250 °C [Tahan, 2022]. This limitation is taken into consideration for the compressors in the flowsheet. Maximum compression ratio is 3, hence if higher pressure ratio is needed, multistage compressors with same pressure ratio at each stage are chosen. Additionally, a typical isentropic efficiency of 0.80 and mechanical efficiency of 0.90 were assumed for the compressors [Ruokonen et al., 2021]. Heat exchangers are simplified in the simulation to streamline the modeling process. Therefore, the *heater/cooler* unit operation is implemented to represent all heat exchangers throughout the process. Distillation column is modelled as RADFRAC [Ruokonen et al., 2021].

Due to lack of information on the isomer distribution, only 1-alkenes up to 24 and n-alkanes up to 24 are considered in the modelling (see Table A.1)

3.2 Methanol Synthesis from CO_2 and H_2

Methanol (MeOH, CH_3OH) is the simplest alcohol molecule, consisting of a single carbon atom with three hydrogen atoms and one hydroxyl group. It is primarily produced via the catalytic hydrogenation of synthesis gas (syngas), a mixture of H_2, CO, and CO_2. Syngas can be produced from a variety of carbon-based feedstocks, such as coal, coke, natural gas, and crude oil; however, natural gas is the most commonly used source due to its availability and favorable hydrogen-to-carbon ratio. [Kaltschmitt and Neuling, 2018, Vandal and Bouallou, 2013]

Methanol synthesis is an exothermic process. The synthesis from CO_2 can be conducted either one-step or two-step process. The one-step approach involves the direct hydrogenation of CO_2 to methanol, whereas the two-step route first converts CO_2 to carbon monoxide (CO) via the Reverse Water-Gas Shift (RWGS) reactor, followed by hydrogenation to methanol. The source of CO_2 can be from flue gases from thermal power plants, or industrial facilities which emits a considerable amount of CO_2. To ensure the sustainability of the process, H_2 should be produced via carbon-free methods, such as production from algae or through water electrolysis powered by renewable electrical sources. [Vandal and Bouallou, 2013]

3.2.1 Model Equations for the Methanol Synthesis

The methanol synthesis reaction is typically carried out over a commercial copper-based catalyst system, commonly composed of $Cu/ZnO/Al_2O_3$, under elevated temperature (210–270°C) and pressures (50-100 bar) [Vandal and Bouallou, 2013]. The conversion of a $CO/CO_2/H_2$ feed into methanol over this catalyst is a well-established process, with different kinetic models proposed in the literature.

The primary reactions responsible for methanol synthesis from syngas are the methanol synthesis reaction and the reverse water-gas shift (RWGS) reaction (eqn. (3.1) and (3.2)). These reactions are highly reversible and gas-phase reactions.

$$CO_2 + 3\,H_2 \rightleftharpoons CH_3OH + H_2O \quad \text{(Methanol Synthesis)} \tag{3.1}$$

$$CO_2 + H_2 \rightleftharpoons CO + H_2O \quad \text{(Reverse Water-Gas Shift)} \tag{3.2}$$

In addition to the primary pathways, two side reactions are included in the based kinetic model to represent the formation of higher alcohols, which are lumped into ethanol and dimethyl ether (DME) (eqn. (3.3), (3.4)). These reactions are generally treated as irreversible, as in this case.

$$2\,CO + 4\,H_2 \longrightarrow C_2H_5OH + H_2O \quad \text{(Ethanol Formation)} \tag{3.3}$$

$$2\,CH_3OH \longrightarrow CH_3OCH_3 + H_2O \quad \text{(DME Formation)} \tag{3.4}$$

The kinetics model for methanol synthesis reaction mechanism is obtained from Aspen Plus documentation which is based on the Vanden Bussche and Froment study [Aspen Technology, Inc., 2021, Bussche and Froment, 1996].

$$r_{\text{MeOH}} = k_{MS} P_{\text{CO}_2} P_{\text{H}_2} \frac{\left(1 - \frac{P_{\text{H}_2\text{O}} P_{\text{CH}_3\text{OH}}}{K_{p,MS} P_{\text{H}_2}^3 P_{\text{CO}_2}}\right)}{\left(K_A + K_B \frac{P_{\text{H}_2\text{O}}}{P_{\text{H}_2}} + K_C P_{\text{H}_2}^{0.5} + K_D P_{\text{H}_2\text{O}}\right)^3} \tag{3.5}$$

$$r_{\text{RWGS}} = k_{RWGS} P_{\text{CO}_2} \frac{\left(1 - \frac{P_{\text{H}_2\text{O}} P_{\text{CO}}}{K_{p,RWGS} P_{\text{CO}_2} P_{\text{H}_2}}\right)}{\left(K_A + K_B \frac{P_{\text{H}_2\text{O}}}{P_{\text{H}_2}} + K_C P_{\text{H}_2}^{0.5} + K_D P_{\text{H}_2\text{O}}\right)} \tag{3.6}$$

where reaction rates (r_{MS} and r_{RWGS}) are in $kmol/kg_{cat}.s$. k_{MS} and k_{RWGS} are rate constants which can be calculated by Arrhenius equation at a specific temperature;

$$k = k_{\text{ref}} e^{-\frac{E_a}{R}\left(\frac{1}{T} - \frac{1}{T_{\text{ref}}}\right)} \tag{3.7}$$

$K_{p,MS}$ and $K_{p,RWGS}$ are equilibrium constants and can be calculated from Gibbs energy;

$$K_p = e^{-\frac{\Delta G^\circ_{rxn}}{RT}} \tag{3.8}$$

K_A, K_B, K_C and K_D are adsorption constants and can be calculated from;

$$ln(K_a) = A + B/T \tag{3.9}$$

The parameter values are given in Table 3.1.

Table 3.1: Kinetic parameters for main reactions (methanol formation and RWGS).

Parameter	Description	Value
$k_{MS,\text{ref}}$	Rate constant for methanol synthesis	7.07034 kmol/kg-cat/s
$E_{a,MS}$	Activation energy for methanol synthesis	-8.76469 kcal/mol
$k_{RWGS,\text{ref}}$	Rate constant for RWGS reaction	0.00165 kmol/kg-cat/s
$E_{a,RWGS}$	Activation energy for RWGS reaction	22.6342 kcal/mol
$K_{p,MS}$	Equilibrium constant for methanol synthesis	Calculated from Gibbs free energy
$K_{p,RWGS}$	Equilibrium constant for RWGS	Calculated from Gibbs free energy
K_A	First adsorption term	$A_A = 0, B_B = 0 \quad (K_A = 1.0)$
K_B	Second adsorption term	$A_A = 8.14711, B_B = 0$
K_C	Third adsorption term	$A_A = -0.69125, B_B = 2066.17$
K_D	Fourth adsorption term	$A_A = -23.4383, B_B = 14928.2$

* Pressure units are implicitly in bar.

For side reactions for ethanol and DME, the exact mechanisms are not well-established, hence the ethanol formation rate is based on a modified power-law expression adapted from Miranda et al., treating the carbon monoxide dependence as first-order, and the DME rate expression is based on the study by Chiang and Lin, which modeled the formation as a second-order reaction with respect to methanol over copper oxide catalysts. [Aspen Technology, Inc., 2021]

$$r_{\mathrm{EtOH}} = k_a P_{\mathrm{CO}}^{x} P_{\mathrm{H_2}}^{y} (W_{\mathrm{cat}} F_{\mathrm{cat}}) \tag{3.10}$$

$$r_{\mathrm{DME}} = k_{\mathrm{DME}} P_{\mathrm{CH_3OH}}^{z} (W_{\mathrm{cat}} F_{\mathrm{cat}}) \tag{3.11}$$

where reaction rates (r_{EtOH} and r_{DME}) are in $kmol/kg_{cat}.s$. k_{EtOH} and k_{DME} are rate constants, which again can be calculated by Arrhenius equation.

The parameters used for these rate expressions are listed in Table 3.2.

Table 3.2: Kinetic parameters for side reactions (ethanol and DME formation).

Parameter	**Description**	**Value**
r_{EtOH}	Rate of ethanol formation	kmol/sec
r_{DME}	Rate of DME formation	kmol/sec
P_x	Partial pressure (for x = H_2, CO, CH_3OH, etc.)	bar
k_a	Forward rate constant for ethanol formation	kmol/kg-cat/s
$k_{a,\mathrm{ref}}$	Reference rate constant for EtOH formation	1.0×10^{-12} kmol/kg-cat/s
E_a	Activation energy for ethanol formation	19.467 kcal/mol
k_{DME}	Forward rate constant for DME formation	kmol/kg-cat/s
$k_{\mathrm{DME,ref}}$	Reference rate constant for DME formation	1.0×10^{-11} kmol/kg-cat/s
E_{DME}	Activation energy for DME formation	18.66 kcal/mol
T_{ref}	Reference temperature	501.57 K (228.42 °C)
x	Power-law exponent for CO	1.0
y	Power-law exponent for H_2	1.5
z	Power-law exponent for CH_3OH	2.0
W_{cat}	Catalyst weight (from reactor model)	–
F_{cat}	Catalyst activity factor (1.0 for fresh)	–

The main reactions, eqn. (3.1) and (3.2), are defined using the Langmuir – Hinshelwood – Hougen – Watson (LHHW) heterogeneous reaction format, while the side reactions, eqn. (3.3) and (3.4), are implemented as irreversible power-law expressions. [Aspen Technology, Inc., 2021]

3.3 Methanol-to-Olefins

Methanol-to-Olefins (MTO) process is the step of the methanol-to-jet (MtJ) fuel production route, in which methanol is catalytically formed into light olefins, mainly ethylene (C_2H_4) and propylene (C_3H_6). The operating conditions of the MTO reactor are about 450-500°C. While higher pressures lead to a higher methanol conversion, lower olefin yield, hence pressures close to atmospheric pressure is more preferred [Eyberg et al., 2024].

Table 3.3: Key modeling parameters of the Methanol-to-Olefins (MTO) process. [Bube et al., 2024]

Model Parameter	**Value**
Operating conditions	$T = 450\,^{\circ}\text{C}$ | $P = 3$ bar
Reaction parameter	Olefin selectivity (S_O) = 90%
Reaction conversion [%]	100
Conversion reactions [%]	
$2CH_3OH \rightarrow C_2H_4 + 2H_2O$	$46.00 \cdot S_O$
$3CH_3OH \rightarrow C_3H_6 + 3H_2O$	$42.89 \cdot S_O$
$4CH_3OH \rightarrow C_4H_8 + 4H_2O$	$11.11 \cdot S_O$
$13CH_3OH \rightarrow 2CO_2 + 9H_2O + 2CH_4 + C_2H_6 + C_3H_8 + C_4H_{10} + H_2$	$(1 - S_O) - 3.81$
$14CH_3OH \rightarrow \text{Coke} + 14H_2O + 3CH_4$	3.81

In this study, the design of MTO unit is based on the UOP/Norsk Hydro MTO process [Bube et al., 2024]. A total methanol conversion of 100% is assumed, and fractional conversions are based on given values scaled with the olefin selectivity (S_O) in Table 3.3. The reactor is modeled using RSTOIC in Aspen Plus. Together with the MTO reactor, regeneration reactor is also modelled for coke combustion after MTO process, where 100% conversion is assumed [Bube et al., 2024].

3.4 Oligomerization

Oligomerization is a process, converting light olefins, primarily ethylene (C_2H_4), propylene (C_3H_6), and butylene (C_4H_8), into longer-chain hydrocarbons desirably within the kerosene boiling range (C8–C_{16}). These oligomerization reactions are typically catalyzed by solid acid catalysts such as zeolites (e.g., ZSM-5 and SAPO-34) under moderate temperature and pressure conditions [Eyberg et al., 2024]. For the formation of hydrocarbons in the jet fuel range, operating conditions are 150-300 °C and 40-100 bar [Bube et al., 2024]. The reactions are exothermic and proceed with a reduction in volume, requiring careful thermal management. The product distribution usually follows the Anderson–Schulz–Flory (ASF) model, which predicts chain growth and favors a wide range of hydrocarbon lengths, including the desirable C8–C16 range [Nicholas, 2017, Bube et al., 2024].

3.4.1 Model Equations for Oligomerization

Oligomerization reactor is modeled as a custom unit integrated into Aspen Plus using MATLAB through an Excel interface. Experimental data from Tabak et al. with ZSM-5 catalyst was used to develop a simple temperature- and pressure-dependent conversion model for C_2-C_4 olefins [Tabak et al., 1986] (see Appendix C). The product distribution of the converted olefins (C_4^+ was assumed to follow the Anderson–Schulz–Flory (ASF) distribution, as seen in eqn. 3.12 as described by Bube et al. [Bube et al., 2024].

$$W_n = (n - x - 1)(1 - \alpha)^2 \alpha^{n-x-2} \quad \text{for } n \geq x \tag{3.12}$$

where W_n is the weight fraction of the paraffin with carbon number n, α is the chain growth probability, and x is an adjustment parameter. In this work, x is set to 2. The value of α governs the likelihood of forming longer hydrocarbon chains: lower α values favor the production of lighter hydrocarbons, while higher α values increase the yield of heavier fractions, potentially resulting in higher wax formation. [Bube et al., 2024]

α value is also correlated with temperature and pressure, with the experimental product distribution data at different temperatures and pressures [Tabak et al., 1986]. To calibrate the ASF distribution, α values are determined by minimizing the error between the model and experimental weight distributions using a "golden section search algorithm". This is a one-dimensional optimization method which finds the minimum of an unimodal function over a bounded interval without taking derivatives. The objective is defined in eqn. 3.13).

Objective: Minimize the squared error between experimental and ASF-predicted weight fractions:

$$f(\alpha) = \sum_{n=3}^{40} \left(W_{\text{exp}}(n) - W_{\text{ASF}}(\alpha, n) \right)^2 \tag{3.13}$$

Subject to:

$$0 \leq \alpha \leq 1$$

The algorithm iteratively calculates the objective function at two interior points within the interval [0,1], chosen based on the golden ratio ($\sim$0.618), and progressively reduces the interval by discarding the side with the higher error. This method is particularly suitable in this case, as the error function is smooth and has a single minimum point with respect to α.

Figure 3.1 shows the model predictions at constant temperature (T = 550 K) and varying pressure, while Figure 3.2 presents results for varying temperature at constant pressure (P=1 bar). Across both cases, the predictions for alpha values generally provides a good fit to experimental carbon distributions, especially at intermediate conditions. The ac-

curacy improves as conversion increases (reflected in higher α), which is evident from the increased alignment of predicted and experimental distributions at higher pressures (e.g., 2–5 bar) and mid-range temperatures (550–600 K). At extreme conditions (high pressures or high temperatures), noticeable discrepancies is observed. Quantitatively, the fitted model achieves high R^2-values ($\sim$ 0.90-0.95) in most cases, with RMSE and MAE values below 0.01. However, at 700 K and 1 bar, as well as at 550 K and 10 bar, the model performance reduces, with corresponding R^2-values of 0.63 and 0.36, respectively. These results suggest that the ASF model struggles to accurately represent product distribution under very high temperature or pressure conditions. Despite these outliers, the overall fit quality confirms that the α predictions combined with ASF logic can reliably capture the oligomer distribution trend across a realistic relevant range of conditions. Furthermore, the observed trend of α increasing with pressure and decreasing with temperature aligns with expected ASF distribution behavior, further supporting the model's validity.

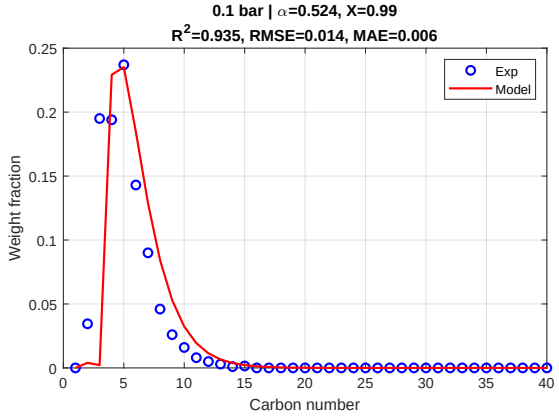

(a) 0.1 bar

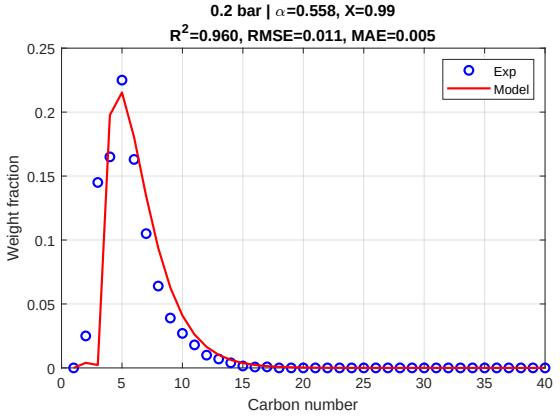

(b) 0.2 bar

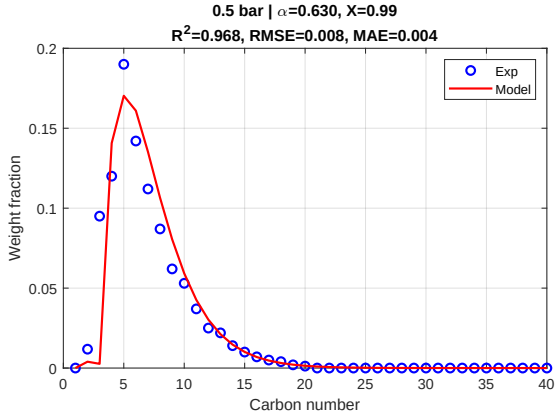

(c) 0.5 bar

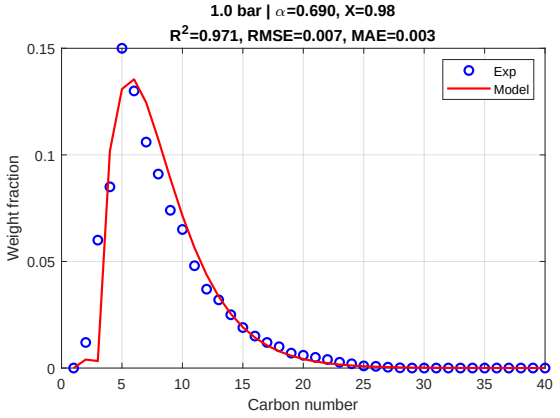

(d) 1.0 bar

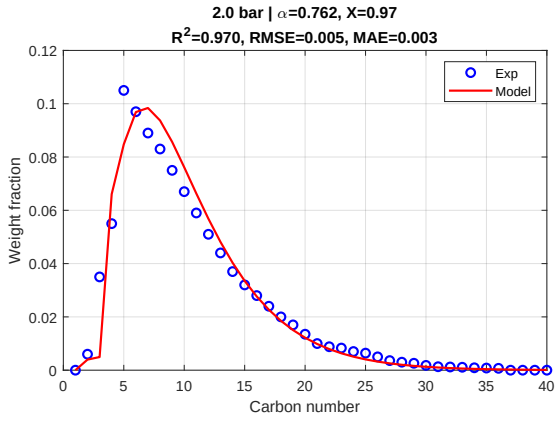

(e) 2.0 bar

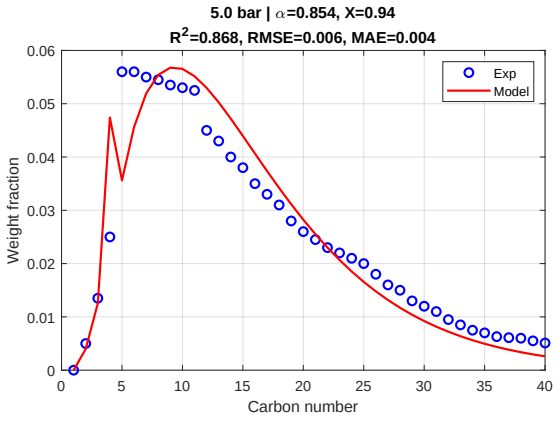

(f) 5.0 bar

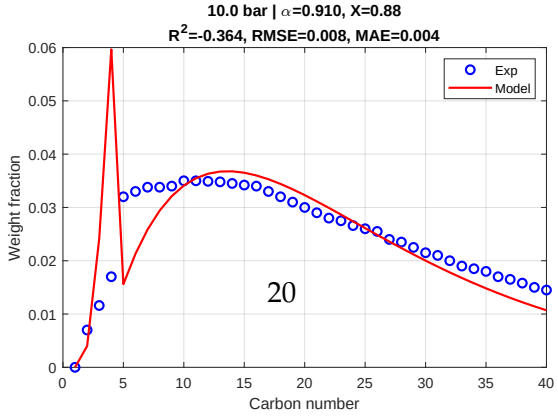

(g) 10.0 bar

Figure 3.1: ASF model predictions vs. experimental data at different partial pressures (PP) of olefins (T = 550 K).

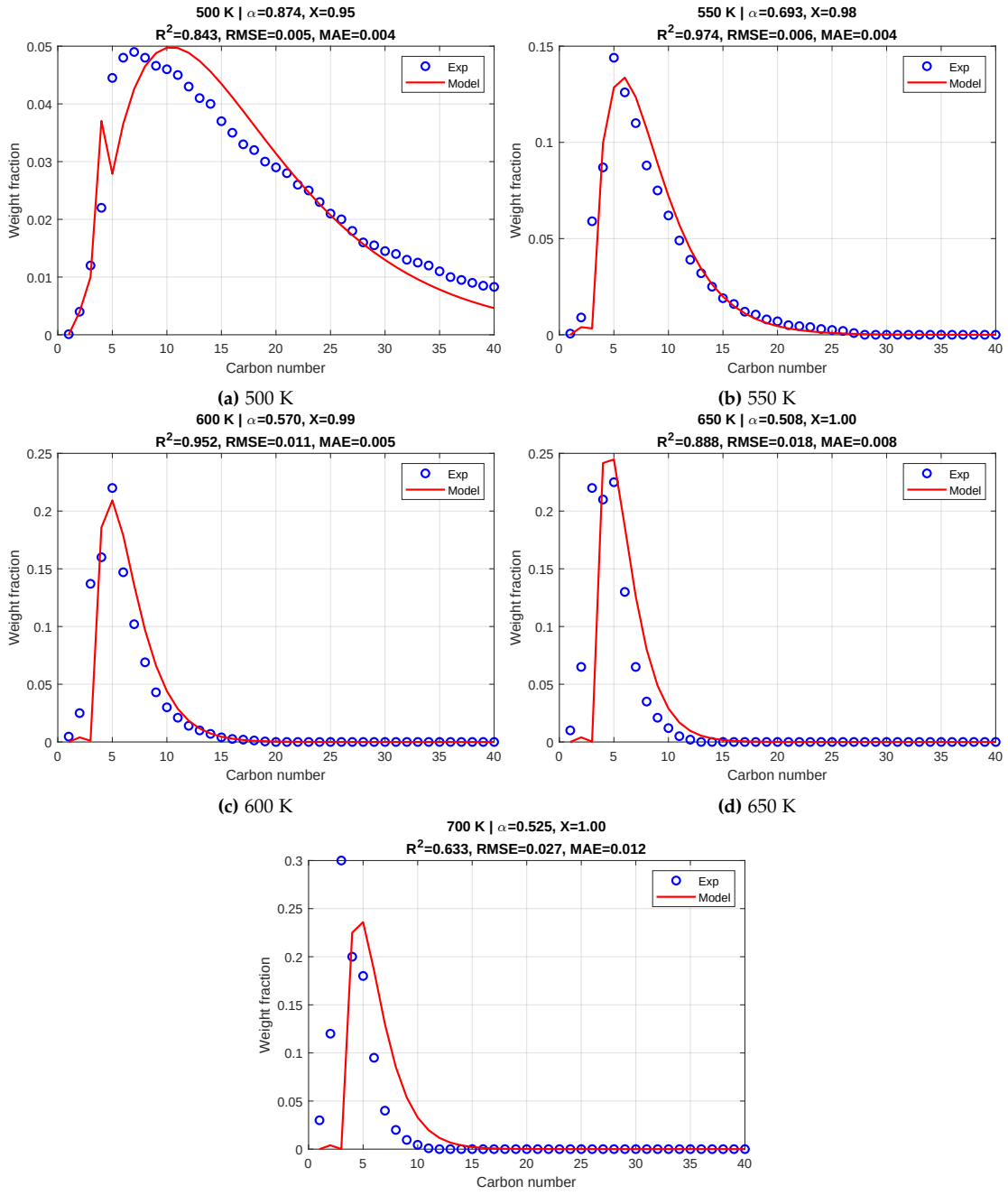

(a) 500 K **(b)** 550 K **(c)** 600 K **(d)** 650 K **(e)** 700 K

Figure 3.2: ASF model predictions vs. experimental data at different temperatures ($PP = 1$ bar).

After predicting α values with the help of experimental data by Tabak et al., in order to enable dynamic prediction of the ASF chain growth probability parameter, α based on reactor conditions, a surface model α(T,P) is developed:

$$\alpha(T, P) = a_0 + a_1 T_n + a_2 P_n + a_3 T_n^2 + a_4 P_n^2 + a_5 T_n P_n \tag{3.14}$$

bounded by;

$$0 \leq \alpha \leq 1$$

where T_n and P_n represent the normalized temperature and pressure values, respectively. The normalization was done using the mean and standard deviation of the dataset. The coefficients a_i were estimated via least squares regression on MATLAB.

Table 3.4: Fitted coefficients for the $\alpha(T, P)$ surface model and corresponding evaluation metrics.

Parameter	**Value**
a_0	0.82
a_1	-0.151
a_2	0.507
a_3	0.026
a_4	-0.168
a_5	0.052
Model Evaluation Metrics	
R^2	0.98
RMSE	0.019
MAE	0.015

As shown in Table 3.4, the fitted model gives a high R-squared value of 0.9809, indicating that it matches the training data well.

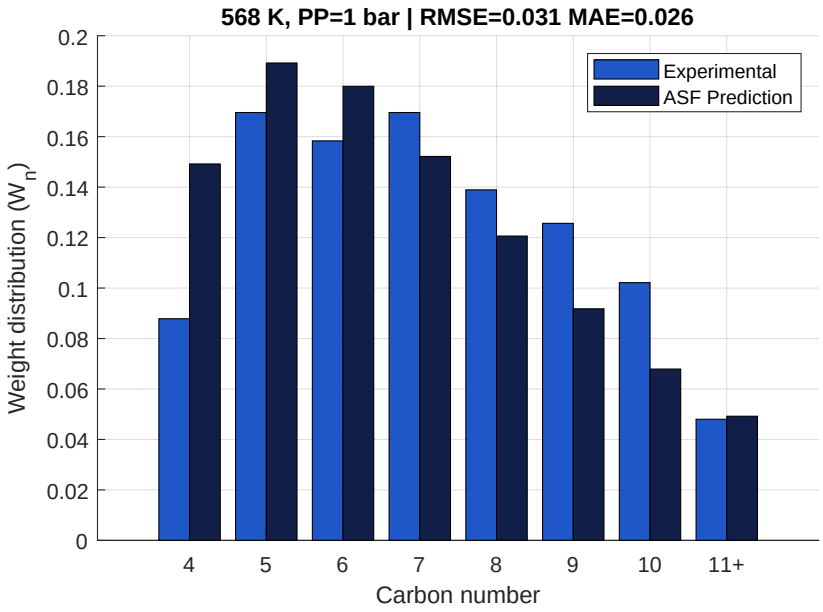

Figure 3.3: Comparison of ASF-predicted and experimental C_4^+ product distributions at 568 K and 1 bar.

In order to assess the general applicability of the ASF model with the α(T,P), it was further validated using the experimental data from Garwood [Garwood, 1983] as testing dataset. As illustrated in Figure 3.3, the ASF model using the fitted α(T,P) surface captures the overall trend in the product distribution across C4 to C11+. The match is especially good in the middle carbon range (C_5–C_8), though there are some deviations at the lower and upper ends. Despite those facts, the RMSE and MAE values of 0.031 and 0.026, respectively, confirm that the model performs quite well, even on data it wasn't originally fitted to.

To enable integration with Aspen Plus, a function was created in MATLAB that combines the ASF product distribution model (eqn. 3.12) with the fitted $\alpha(T, P)$ surface model (Equation 3.14). This function calculates the expected weight distribution of oligomerization products based on given inlet temperature and partial pressure of olefin reactants, using the predicted chain growth probability α. The output from this MATLAB routine is then dynamically linked to the Aspen simulation through Excel, allowing the user-defined model to interact with the overall process flowsheet in Aspen.

Aspen Plus–Excel–MATLAB Dynamic Data Exchange Overview

In order to simulate the distribution of the oligomerization product considering the effect of temperature and pressure with the experimental data, a custom unit in Aspen is used. When built-in unit operation models are insufficient, integrating a custom MATLAB model which captures the behavior of the reactor outlet can be an option.

In this perspective, the Dynamic Data Exchange (DDE) approach provides a mechanism to link Aspen Plus with external software (Excel and MATLAB) at runtime, allowing data to be passed back and forth between the Aspen simulation and a user-defined calculation (see Figure 3.4) [Fontalvo, 2014]. Aspen Plus serves as the primary flowsheet simulator, Excel acts as a data channel and automation platform, and MATLAB has the custom model. This setup enables Aspen to utilize MATLAB's computational power with updating the Aspen environment simultaneously. The logic for this approach is to preserve Aspen's robust features (thermodynamics, unit operation network, and convergence routines) while incorporating calculations from MATLAB.

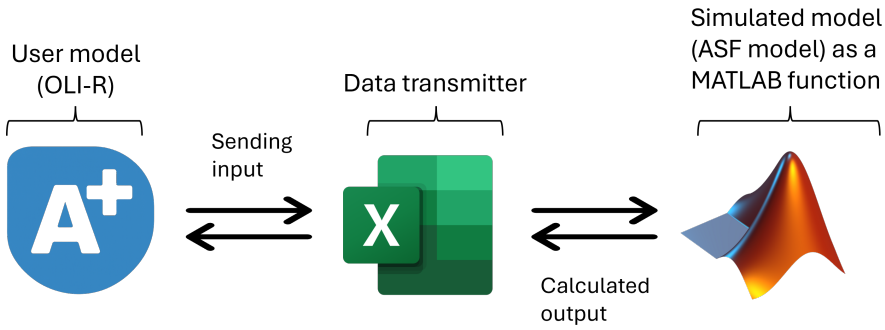

Figure 3.4: Matlab-Excel-Aspen Dynamic Data Exchange.

- **Aspen Plus User Model Block:** Aspen Plus provides a "User Model" unit operation (User2 block) which can accept one or more inlet streams and produce one or more outlet streams, and it allows the user to specify an external subroutine to compute the outlet stream conditions. In this case, this subroutine is an Excel workbook, as opposed to a FORTRAN routine, which also interfaces with MATLAB. Hence, this User2 block functions as custom reactor for oligomerization of light olefins process.

- **Excel as Data Bridge:** Excel serves as the data transmitter between Aspen and MATLAB. Aspen Plus uses dynamic data exchange to push simulation data into specific cells of an Excel workbook, and to retrieve results from designated cells after computation. The Excel workbook provided by AspenTech as a template contains a predefined function in VBA called *Aspenhooks* that send and recieve information to and from MATLAB. Excel's role is reading the feed values from Aspen, calling the MATLAB function with those inputs with the help of Aspenhooks, and then writing the returned results back to the worksheet cells.

- **MATLAB Custom Model Function:** MATLAB contains the actual user-defined model, an ASF-based oligomerization model in this case. It is implemented as a function file. The Excel macro calls MATLAB, passes the necessary inputs, and executes this MATLAB function. There are a couple of ways to do this: one common method is using Excel's VBA (Visual Basic for Applications) to start a MATLAB automation server

(using COM/ActiveX) and call the function, capturing the outputs [Fontalvo, 2014]. Another approach is the use of MATLAB's Spreadsheet Link (Excel add-in of MATLAB) which allows Excel to directly call MATLAB functions via worksheet formulas or VBA. In either case, Excel acts as the client that requests MATLAB to perform a calculation and then retrieves the results. In this study, MATLAB's Spreadsheet Link is used. This step is crucial – it's where the custom model logic (which Aspen itself cannot natively do) is executed. By the time the MATLAB function finishes, the desired output data (e.g. predicted weight distribution of the oligomerization products) are now stored in Excel, ready for Aspen to read.

Through this integrated workflow, Aspen Plus can dynamically simulate a user-defined MATLAB model during its calculations. The Aspenhooks module handles the communication between Aspen and Excel, hence Aspen's data and the Excel cells stay synchronized. On the other hand, the MATLAB Excel Add-In (Spreadsheet Link) handles the communication between Excel and MATLAB, hence Excel delegates complex calculations to MATLAB and get the results back. This three-software setup allows for the dynamic integration of a MATLAB model within an Aspen Plus simulation.

3.5 Hydrogenation

Hydrogenation is used to saturate alkenes produced during oligomerization into alkanes by adding hydrogen, hence enhancing the fuel's chemical stability and storage properties and fitting to jet fuel properties. Hydrogenation is typically catalyzed by metal catalysts such as nickel (Ni), platinum (Pt), or palladium (Pd), often supported on activated carbon. Under standard conditions, noble metal catalysts like Pt, Pd, or PtO_2 can achieve effective hydrogenation, while more robust operating conditions are necessary for less active catalytic systems such as Ni or Co catalysts.

At the industrial scale, cost-effective Raney-nickel catalysts are commonly employed [Kaltschmitt and Neuling, 2018]. These reactions are typically carried out at temperatures ranging from 150–200 °C and pressures between 20 and 40 bar to ensure complete saturation of olefinic compounds.

In this study, the hydrogenation reactor is modelled as RSTOIC reactor and the conversion is assumed to be 99%.

Chapter 4

Process Design Results and Optimization

4.1 Base Case Scenario

4.1.1 Flowsheet Description

CO_2 is initially supplied at 1 bar and H_2 at 30 bar, both at a temperature of 25 °C. The CO_2 stream is compressed to 75 bar using a series of compressors with intercooling between stages, while the hydrogen stream is pressurized to the same pressure in a single compression step [Vandal and Bouallou, 2013]. The methanol synthesis (MEOH-R) is done by a packed bed reactor at isothermal conditions with the given kinetic model in Chapter 3 which is modeled by heterogenous RPLUG reactor in Aspen Plus. The pressure drop in the fixed bed is calculated by the Ergün equation, already implemented inside the software.

The stream exiting the first flash drum (V-100), referred to as crude methanol, consists primarily of methanol, ethanol, DME and traces of dissolved gases, and water is knocked out in this VLLE column. The vapor stream is sent to recycle for further conversion of non-reacted gases to methanol. After that, most of the residual gases are separated in the next flash tank (V-101) and purified methanol is collected from the bottom in liquid form. This stream which mainly consists of methanol is supplied into methanol-to-oligomerization reactor (MTO-R) at 3 bar and 450 °C [Bube et al., 2024]. During this process, coke is included in the reaction scheme, hence, catalyst needs to be regenerated in REGEN-R at adiabatic conditions. The process until this point is given in Figure 4.1.

The water from the product stream of MTO-R is knocked down in the flash tank (V-102). Then the oligomerization into higher olefins occurs in the reactor (OLI-R) at 40 bar and 200 °C. The OLI-R product is then pre-heated to 300 °C to be fed into hydrogenation unit (HYDRO-RS) with hydrogen side stream. Here, the oligomerized olefins are saturated into paraffins. Then the outlet stream is separated in flash column (V-103) into light products, predominantly light alkenes, water and the main stream which is sent to another flash column (V-104) to obtain processed e-crude. Finally, this processed e-crude is fractionated into light cut, kerosene and heavy cut (KERCOL). During fractionation, T10 and final boiling requirements is taken into account as mentioned in Ch. 1. This section is given in Figure 4.2.

The unit specifications for the base scenarios are given in Table 4.1 and 4.2.

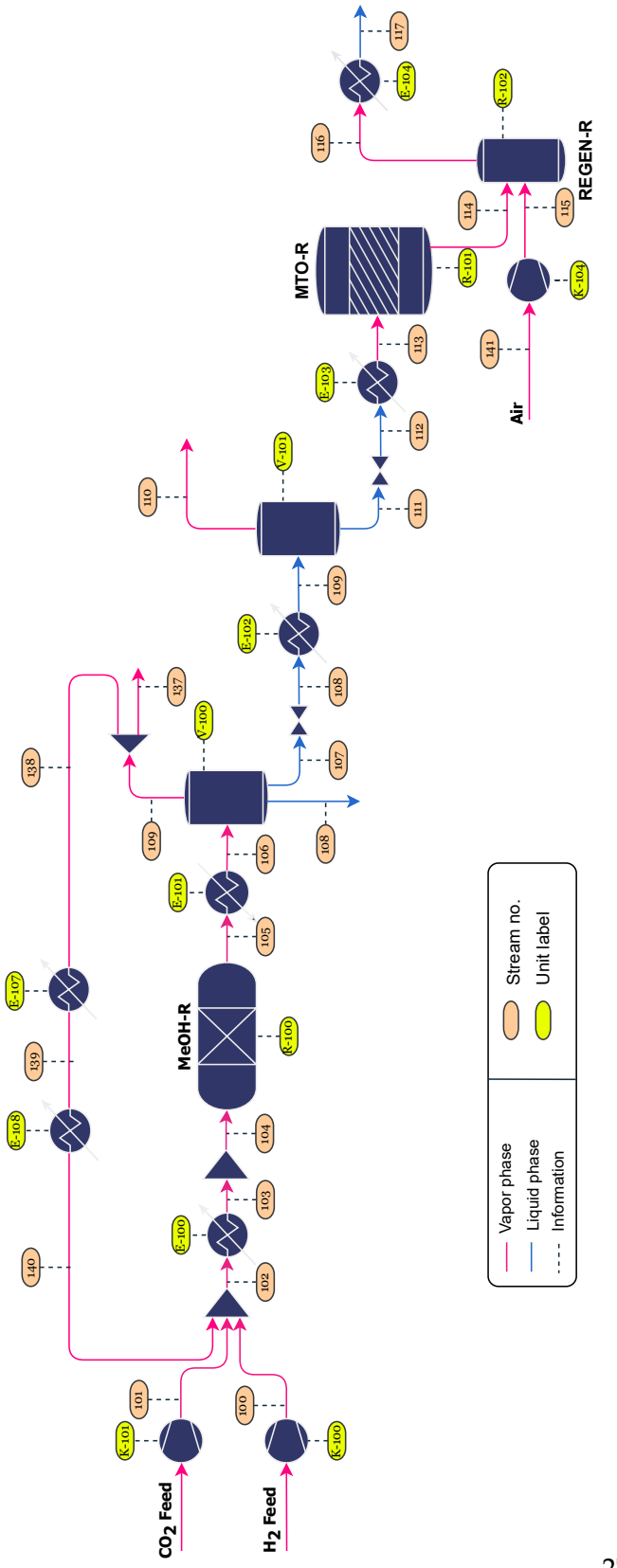

Figure 4.1: Process flow diagram of Part A of the MtJ process.

Table 4.1: Process unit base conditions for Part A of the MtJ process.

Unit no.	K-100	K-101	E-100	R-100	E-101	V-100	E-102	V-101
Description	Compressor (H_2 feed)	Compressor (CO_2 feed)	Pre-heater before MeOH-R	Methanol synthesis reactor (MeOH-R)	MeOH-R outlet cooler	Flash drum (MeOH separation)	Heater after flash	Pre-MTO flash drum
Temperature [°C]	137	250	200	220	35	-	60	-
Pressure [bar]	75	75	75	75	75	75	3	3
Duty [10^5 kJ/h]	0	-21.3	3.6	-52.0	-215.0	0	13.0	0
Work [kW]	409.2	1131.2	-	-	-	-	-	-
Unit no.	E-103	R-101	K-104	R-102	E-104	E-107	E-108	
Description	MTO pre-heater	MTO reactor	Compressor (air feed)	Catalyst regenerator	Cooler after regenerator	Recycle heater	Recycle heater	
Temperature [°C]	450	450	161	553	250	100	180	
Pressure [bar]	3	3	3	3	3	75	75	
Duty [10^5 kJ/h]	65.7	-20.4	0	0	-85.2	33.8	38.4	
Work [kW]	-	-	11.8	-	-	-	-	

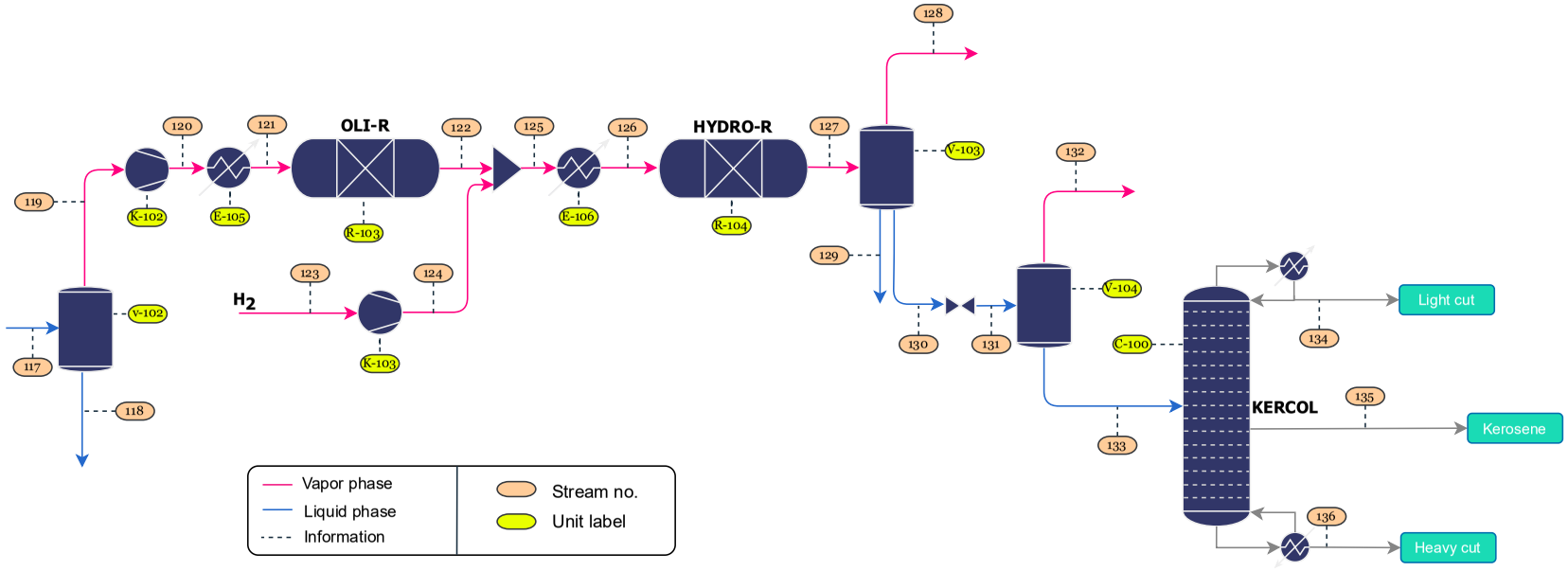

Figure 4.2: Process flow diagram of Part B of the MtJ process.

Table 4.2: Process unit base conditions for Part B of the MtJ process.

Unit no.	V-102	K-102	E-105	R-103	K-103	E-106	R-104	V-103
Description	Flash drum before oligomerization	Compressor before OLI-R	Pre-cooler before OLI-R	Oligomerization reactor (OLI-R)	Compressor (H_2 feed)	Hydrogenation pre-heater	Hydrogenation reactor (HYDRO-R)	Flash drum after hydrogenation
Temperature [°C]	50	240	200	200	68	300	300	135
Pressure [bar]	1	40	40	40	40	40	40	40
Duty [10^5 kJ/h]	-	-4.9	-1.7	-1.5	0	6.6	-10.8	-
Work [kW]	-	344.1	-	-	2.4	-	-	-
Unit no.	V-104	C-100						
Description	Flash drum before distillation	Distillation column (KERCOL)						
Temperature [°C]	70	-						
Pressure [bar]	1	-						
Duty [10^5 kJ/h]	-	Condenser: -3.3 Reboiler: 5.2						
Work [kW]	-	-						

4.2 Optimization Strategy

4.2.1 Response Surface Modeling

In this work, to optimize the MtJ fuel process for minimum capital cost and maximum kerosene yield, a Central Composite Design (CCD) was used to collect simulation data, which was then analyzed using Response Surface Methodology (RSM) to develop a quadratic model for further process optimization. A CCD is a response surface design that combines a factorial core with center and axial (star) points to capture curvature [NIST/SEMATECH, 2012].

The key process variables, methanol synthesis operating pressure, oligomerization operating temperature, and pressure are selected as three factors to vary:

- x_1: MeOH-R pressure (50 – 100 bar)
- x_2: Oligomerization reactor temperature (150 – 300 °C)
- x_3: Oligomerization reactor pressure (40 – 100 bar)

Kerosene yield is defined as;

$$Y_{\text{yield, C8-16}} = \frac{\dot{n}_{\text{C,C8-16 hydrocarbons}}}{\dot{n}_{\text{C,feed}}} \tag{4.1}$$

Using a CCD allows us to fit a full quadratic model (including interactions and squared terms) for both objectives [Minitab, 2025]. The face-centered CCD ($\alpha = 1$) is chosen, so that all experimental runs stay within the given factor ranges; that is, each factor is tested at three levels: low (–1), center (0), and high (+1). In a face-centered design, the axial (star) points are located at the center of each face of the factorial cube (i.e. at the midpoints of the ranges) as seen in Figure 4.3.

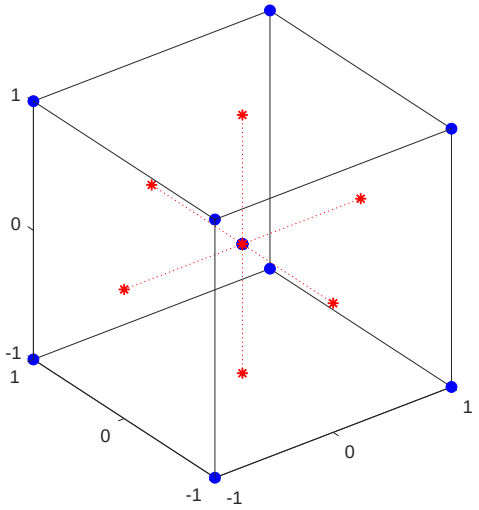

Figure 4.3: Face centered composite design structure.

The total number of runs can be calculated by:

$$N = 2^k + 2k + n_c \tag{4.2}$$

where k is the number of factors and n_c is the number of center point repeats.

The CCD consists of three sets of points:

- **Factorial points:** All combinations of factors at low and high levels. These cover the "corners" of the design space and capture main effects and interactions in a linear model. For the case of this study which consists of 3 factors, factorial points correspond to 2^3 = 8 runs (blue dots in Figure 4.3).
- **Axial (star) points:** One-factor-at-a-time extremes, with others at center. These points (coded as ±1 for one factor, 0 for the others) lie at the midpoints of each face of the cube and allow estimation of curvature (quadratic effects) for each factor. In this case, they are 2x3 = 6 runs in total (red stars in Figure 4.3).
- **Center points:** Runs where all factors are at the midpoint of their ranges (coded as 0,0,0). Number of center runs depend on the replication of the experiment. In this case, no repetition is needed, hence 1 run (overlapped point at the center in Figure 4.3).

These add up to 15 runs in total, where the results are shown in Table 4.3.

Table 4.3: Central Composite Design Matrix and Simulation Results.

Run	P_{MeOH} [bar]	T_{OLI} [°C]	P_{OLI}[bar]	P_{MeOH} (coded)	T_{OLI} (coded)	P_{OLI} (coded)	C-mole Yield of Kerosene defined as C8-16 [-]	Capital Cost [mil. EUR]
1	30.0	150	40	-1	-1	-1	0.2694	23.75
2	30.0	150	70	-1	-1	1	0.2047	24.22
3	30.0	300	40	-1	1	-1	0.3356	23.50
4	30.0	300	70	-1	1	1	0.4100	24.53
5	75.0	150	40	1	-1	-1	0.2580	28.98
6	75.0	150	70	1	-1	1	0.1951	32.09
7	75.0	300	40	1	1	-1	0.3320	31.16
8	75.0	300	70	1	1	1	0.3949	32.21
9	30.0	225	55	-1	0	0	0.3571	23.91
10	75.0	225	55	1	0	0	0.3463	31.52
11	52.5	150	55	0	-1	0	0.2208	26.64
12	52.5	300	55	0	1	0	0.3816	26.39
13	52.5	225	40	0	0	-1	0.3444	25.93
14	52.5	225	70	0	0	1	0.3249	28.42
15	52.5	225	55	0	0	0	0.3448	26.53

RSM provides a statistical and mathematical framework for modeling the relationship between a response variable (output) and multiple design variables (factors). The main objective is to approximate the true functional relationship between the factors and the response in a given data and use this to identify optimal conditions [Montgomery, 2017]. A typical RSM model takes the form:

$$y = f(x_1, x_2, \ldots, x_k) + \varepsilon \tag{4.3}$$

where ε represents experimental noise or error. If the surface is approximately linear, a first-order model may suffice:

$$y = \beta_0 + \sum_{i=1}^{k} \beta_i x_i + \varepsilon \tag{4.4}$$

However, if curvature exists in the response surface, a second-order polynomial model is employed:

$$y = \beta_0 + \sum_{i=1}^{k} \beta_i x_i + \sum_{i=1}^{k} \beta_{ii} x_i^2 + \sum_{i<j} \beta_{ij} x_i x_j + \varepsilon \tag{4.5}$$

where x are factors and y is the predicted response. This model allows for the estimation of linear, interaction, and quadratic effects of each factor. In practical, in most of the RSM problems, linear or second-order polynomial models (eq. 4.4, 4.5) are used. Although a polynomial model is unlikely to be a good representation of the true functional relation-

ship across the whole space of the independent variables, they typically perform well for a relatively small range [Montgomery, 2017].

The responses (kerosene yield and capital cost) are normalized to [0, 1] using min-max scaling to ensure equal weighting during fitting and MATLAB's `fitlm` is used to fit the response surface models.

The fitting RSM curves are given in the following (see Figure 4.4).

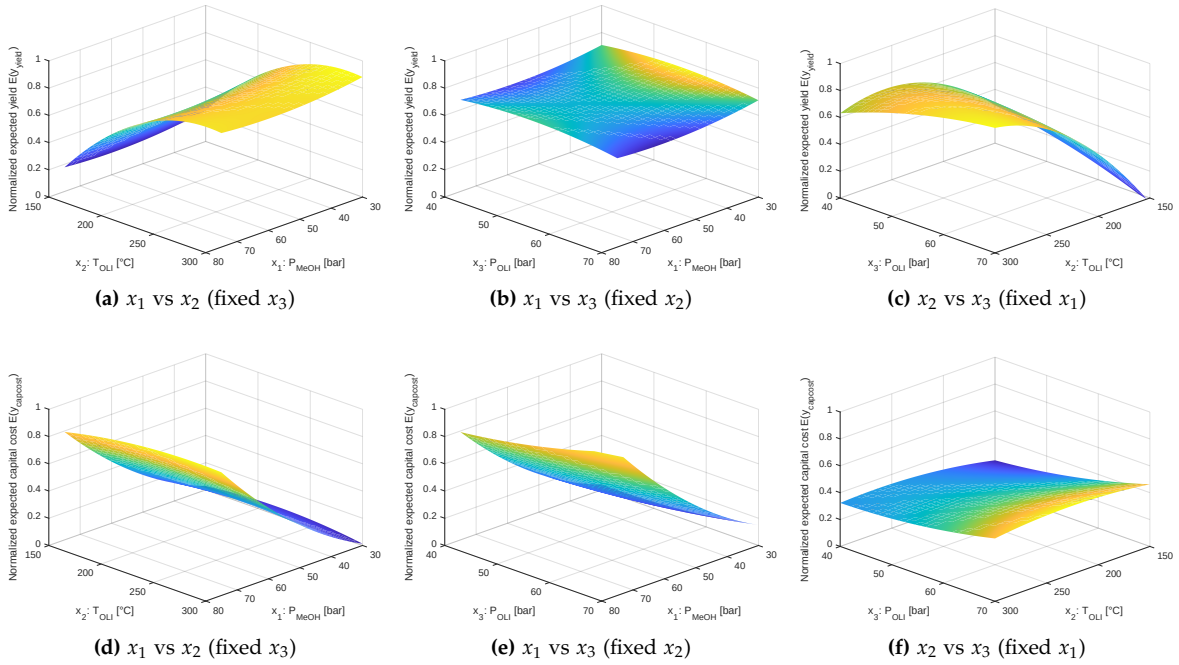

(a) x_1 vs x_2 (fixed x_3) **(b)** x_1 vs x_3 (fixed x_2) **(c)** x_2 vs x_3 (fixed x_1)

(d) x_1 vs x_2 (fixed x_3) **(e)** x_1 vs x_3 (fixed x_2) **(f)** x_2 vs x_3 (fixed x_1)

Figure 4.4: Response surfaces for (top) normalized expected kerosene yield $E(y_{\text{yield}})$ and (bottom) expected capital cost $E(y_{\text{capcost}})$ as functions of selected factor pairs. The third factor is held at its midpoint in each case.

Analysis of variance (ANOVA) results for the response surface model of normalized kerosene yield and capital cost are given in Tables 4.4 and 4.5, respectively. All significance tests were conducted at a 95% confidence level ($\alpha = 0.05$).

Table 4.4: ANOVA summary for the RSM of normalized kerosene yield.

Source	SSE	DF	MSE	F	p-Value
Total	1.4267	14	0.10191		
Model	1.4169	9	0.15743	79.99	7.2315e–05
Linear	1.0852	3	0.36175	183.82	1.5542e–05
Nonlinear	0.33166	6	0.05528	28.09	0.0010647
Residual	0.00984	5	0.001968		
R^2 values			Adjusted = 0.99		
			Adjusted = 0.98		

The ANOVA results for normalized kerosene yield indicate that the model is statistically significant at the 95% confidence level ($F = 79.997$, $p = 7.23 \times 10^{-5}$). Most of the variation is captured by the linear terms ($F = 183.82$, $p = 1.55 \times 10^{-5}$), but the nonlinear terms are also significant ($F = 28.088$, $p = 0.00106$), which confirms that curvature is present in the response surface. The residual error is very low, and the model gives a high R^2 value of 0.99 and an adjusted R^2 of 0.98, meaning the model fits the data very well without overfitting.

Table 4.5: ANOVA summary for the RSM of normalized capital cost.

Source	SSE	DF	MSE	F	p-Value
Total	1.8894	14	0.13495		
Model	1.8657	9	0.20730	43.87	3.153e–04
Linear	1.8078	3	0.60261	127.54	3.8322e–05
Nonlinear	0.05790	6	0.00965	2.042	0.22521
Residual	0.02363	5	0.004725		
R^2 values			Ordinary = 0.99		
			Adjusted = 0.96		

Similarly, for the capital cost RSM, the total model is also significant ($F = 43.874$, $p = 3.15 \times 10^{-4}$). The linear terms dominate the model, explaining most of the response variation ($F = 127.54$, $p = 3.83 \times 10^{-5}$), whereas the nonlinear terms are not statistically significant ($F = 2.0425$, $p = 0.225 > 0.05$). This suggests that a linear approximation might be sufficient in this case. The model still performs well, with $R^2 = 0.99$ and adjusted $R^2 = 0.97$. After fitting the response surfaces for both kerosene yield and capital cost, the next step is to determine optimal trade-offs between cost and yield.

4.2.2 Optimization Problem Formulation

Objectives and Normalization

The optimization problem involves finding the best combination of process conditions, which are the design variables defined in the previous section, to maximize kerosene yield and minimize capital cost.

The multi-objective optimization problem can be formulated as:

$$minimize \begin{Bmatrix} f_1(\mathbf{x}) \\ f_2(\mathbf{x}) \end{Bmatrix} = \begin{Bmatrix} -\text{Kerosene yield} \\ \text{Capital cost} \end{Bmatrix}$$

where f_1 is the kerosene yield RSM and f_2 is the capital cost RSM. The minus sign in f_1 reflects that yield needs to be maximized.

bounded by;

$$30 \leq x_1 \leq 75 \text{ bar}$$

$$150 \leq x_2 \leq 300 \text{ }^{\circ}\text{C}$$

$$40 \leq x_3 \leq 70 \text{ bar}$$

Genetic Algorithm

A multi-objective genetic algorithm (GA) was used to generate the Pareto front, implemented using MATLAB's `gamultiobj` with population size of 300 and 250 generations. The objective function returns normalized predictions from the response surface models. The GA searched for Pareto-optimal solutions that represent a balance between the two conflicting objectives. GAs offer the advantage of identifying not just a single optimum but a diverse set of nondominated solutions. These solutions form the Pareto front, which consists of points for which no objective can be improved without worsening another. A solution is considered Pareto optimal if no other feasible solution exists that improves one objective without degrading at least one other. [Arora, 2016]

Pareto Front and Knee-Point Selection

Figure 4.5 shows the Pareto front generated from the multi-objective genetic algorithm, where normalized kerosene yield is plotted against normalized capital cost. Each black point represents a nondominated solution, meaning no point offers a better yield without increasing cost, and vice versa. To select a compromise operating point, the knee point is identified, which is the solution closest to the ideal (utopia) point of maximum yield and minimum cost. This is done by minimizing the Euclidean distance in the objective space.

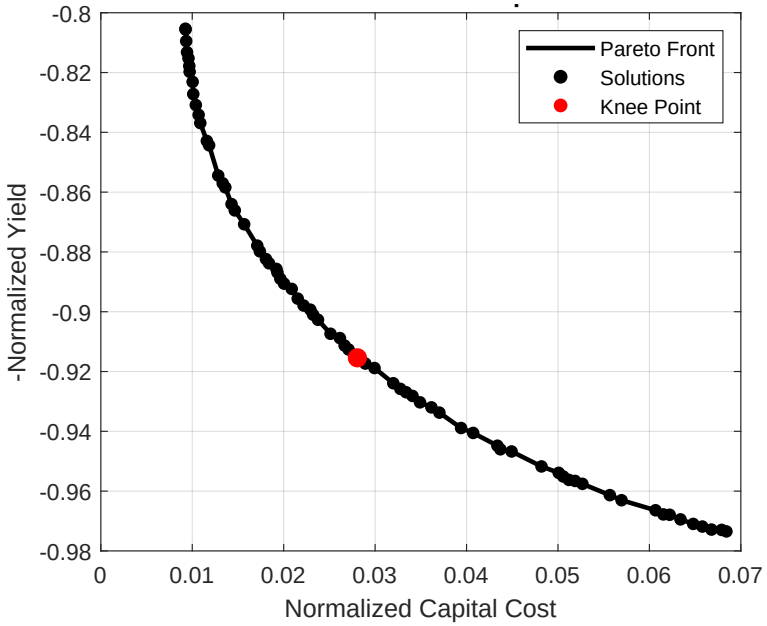

Figure 4.5: Pareto front showing normalized kerosene yield vs. capital cost. The red point indicates the selected knee solution.

With the combination of RSM and multi-objective optimization, the optimal operating conditions for yield and cost are determined (see Table 4.6).

Table 4.6: Optimization results.

Parameter	**Value**
P_{MeOH}	30.0 bar
T_{OLI}	299.9°C
P_{OLI}	59.6 bar

4.2.3 Simulation Results with the Optimum Inputs

Targeting reduced capital cost and improved kerosene yield, the simulation is run again with the optimized operating conditions mentioned before. Table 4.7 demonstrates the expected results and actual simulation results. Comparing the results with Table 4.3, it can be interpreted that the algorithm successfully identified a design point that was not part of the original simulations but still yielded an improved trade-off.

Table 4.7: Comparison of expected values from optimization and actual simulation results at the selected knee point.

Output	Expected (RSM) Value	Simulation Results
Kerosene yield [Cmole/Cmole]	0.394	0.400
Capital cost [mil. €]	23.73	23.67

The yield, 0.400 Cmole/Cmole is among the highest across all simulations, only slightly lower than Run 4 (0.410) in Table 4.3. However, it results in significantly less capital cost than other high-yield cases such as Run 4 (24.53 mil.€) or Run 8 (32.21 mil.€). On the other hand, while in the case of Run 3 (23.50 mil.€), capital cost is lower, but it has lower yield (0.336).

In general terms, the results confirm that the optimization routine was able to interpolate beyond the discrete DOE points and locate a new operating condition with a more favorable balance between economic and performance objectives.

4.3 Optimized Case Scenario

In the optimized scenario, the kerosene yield increased to 3945 tonnes/hr compared to 2103 tonnes/hr in the base case. The updated unit specifications for the optimized scenario are presented below:

Table 4.8: Optimized process unit conditions for Part A of the MtJ process.

Unit no.	K-100	K-101	E-100	R-100	E-101
Description	Compressor (H_2 feed)	Compressor (CO_2 feed)	Pre-heater before MeOH-R	Methanol synthesis reactor (MeOH-R)	MeOH-R outlet cooler
Temperature [°C]	*Deleted*	30	200	220	35
Pressure [bar]	*Deleted*	189	30	30	30
Duty [10^5 kJ/h]	*Deleted*	-13.8	21.5	-27.02	-290.8
Work [kW]	*Deleted*	773.9	-	-	-
Unit no.	V-100	E-102	V-101	E-103	R-101
Description	Flash drum (MeOH separation)	Heater after flash	Pre-MTO flash drum	MTO pre-heater	MTO reactor
Temperature [°C]	-	60	-	200	450
Pressure [bar]	30	3	3	3	3
Duty [10^5 kJ/h]	0	6.8	0	63.3	-19.8
Work [kW]	-	-	-	-	-
Unit no.	K-104	R-102	E-104	E-107	E-108
Description	Compressor (air feed)	Catalyst regenerator	Cooler after regenerator	Recycle heater	Recycle heater
Temperature [°C]	161	554	50	102	185
Pressure [bar]	3	3	3	30	30
Duty [10^5 kJ/h]	0	0	-82.6	80.5	61.8
Work [kW]	11.5	-	-	-	-

Table 4.9: Optimized process unit conditions for Part B of the MtJ process.

Unit no.	V-102	K-102	E-105	R-103	K-103
Description	Flash drum before OLI-R	Compressor before OLI-R	Pre-heater before OLI-R	Oligomerization reactor (OLI-R)	Compressor (H_2 feed)
Temperature [°C]	50	250	300	300	68
Pressure [bar]	1	60	60	60	40
Duty [10^5 kJ/h]	–	-5.8	2.2	-22.4	0
Work [kW]	–	370.5	–	–	3.0
Unit no.	E-106	R-104	V-103	V-104	C-100
Description	hydrogenation pre-heater	Hydrogenation reactor (HYDRO-R)	Flash drum after hydrogenation	Flash drum before distillation	Distillation column (KERCOL)
Temperature [°C]	300	300	94	–	–
Pressure [bar]	40	40	40	1	–
Duty [10^5 kJ/h]	1.2	-13.1	–	0	Condenser: -2.6 Reboiler: 6.0
Work [kW]	–	–	–	–	–

Comparing the base and optimized processes for Part A (Tables 4.1 and 4.8), the first significant difference is the elimination of the hydrogen feed compressor (K-100), as the specified inlet pressure for MeOH-R and the hydrogen from the electrolyzers are both 30 bar. Additionally, the CO_2 compressor (K-101) operates at a much lower pressure in the optimized case, corresponding to approximately 70% compression work of the base case. On the other hand, the duty of the MeOH-R preheater (E-100) increased significantly. This is mainly because the temperatures are not elevated in the feed streams due to very high compression, as in the case of the base case scenario. The methanol reactor (R-100) requires approximately half the cooling duty, as the lower conversion in the optimized case produces less heat. This reduced reactor heat removal is consistent with the increased duties of the recycle heaters (E-107 and E-108), indicating a higher amount of unreacted gases being recycled.

In Part B (Table 4.2 and Table 4.9), the oligomerization reactor (OLI-R, R-103) operates at elevated conditions, with pressure increased from 40 to 60 bar and temperature from 200 to 300 °C. These changes are aimed at optimizing oligomer yields in favor of the kerosene range. Despite the higher compression requirement due to high operating pressure (60 instead of 40 bar), the compressor before OLI-R (K-102) work remained manageable, which changed from 344.1 to 370.5 kW. The higher temperature and pressure result in greater conversion and since oligomerization is an exothermic process, more heat needs to be removed. This trend is also observed in the increased compressor work for the hydrogen feed to the HYDRO-R unit. Meanwhile, the duty of the hydrogenation preheater (E-106) was reduced significantly, from 6.6 to 1.2 $\times$ 10^5 kJ/h, due to the elevated temperature of the product stream exiting OLI-R.

The results of the carbon efficiency and kerosene yield calculations for both the base and optimized scenarios of the MtJ process are illustrated in Figure 4.6. Here, the kerosene yield labeled as $Y_{\text{yield, C8-16}}$ is defined in eqn. (4.1). η_{carbon} is carbon efficiency for raw crude which is the outlet stream of the hydrogenation reactor, HYDRO-R and processed crude is the stream after two flash columns, V-103 and V-104. η_{carbon} is defined in eqn. (4.6);

$$\eta_{\text{C}} = \frac{\dot{n}_{\text{C,hydrocarbons}}}{\dot{n}_{\text{C,feed}}} \tag{4.6}$$

The carbon efficiencies are given in terms of the number of moles of carbons in hydrocarbon products to the number of moles of the reactants (CO_2 and CO) at the inlet. The efficiencies are calculated to indicate how much reactant is converted into hydrocarbons over the process simulation, before flash separation and after.
$Y_{\text{yield, kerosene-cut}}$ is defined in equation (4.7):

$$Y_{\text{yield, kerosene-cut}} = \frac{\dot{n}_{\text{C,hydrocarbons}}}{\dot{n}_{\text{C,feed}}} \tag{4.7}$$

In this case, all the hydrocarbons at the kerosene stream which is obtained from the fractionation unit (KERCOL) are accounted into the calculation contrary to $Y_{\text{yield, C8-16}}$ (eqn. (4.1))

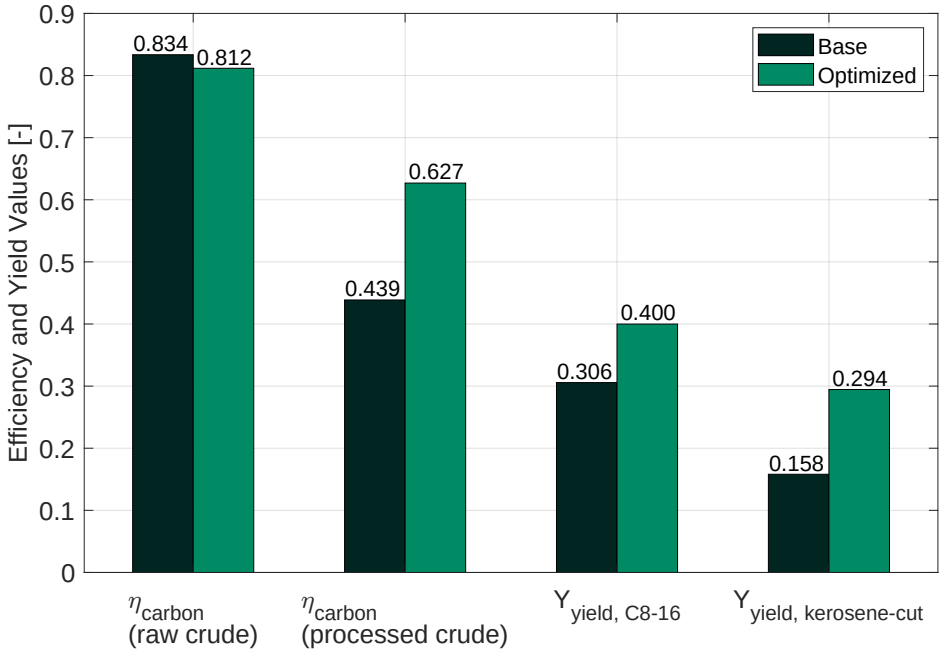

Figure 4.6: Comparison of carbon efficiency and kerosene yield between the base and optimized scenarios.

In Figure 4.6, it can be observed that the raw crude carbon efficiency is slightly higher in the base case. However, both the processed crude carbon efficiency and the kerosene yields are notably improved in the optimized scenario. The higher raw crude efficiency in the base case may be attributed to a greater proportion of light hydrocarbons in the e-crude, which are subsequently removed during separation via the flash columns. In addition to that, the production rate is risen up to 9395 tonnes/year from 2103 tonnes/year which shows a big improvement. Overall, these results indicate that the process performance was successfully enhanced through optimization, particularly in terms of kerosene production, its selectivity and carbon utilization within the targeted kerosene range.

Chapter 5

Techno-Economic Assessment

This chapter presents the techno-economic evaluation of the Methanol-to-Jet (MtJ) process developed in this study. The aim is to assess the financial viability of the proposed pathway under current and projected economic conditions. Key assumptions regarding capital and operating expenditures, cost indices, and financial parameters are outlined, followed by the calculation of levelized cost of sustainable aviation fuel (LCOSAF) to provide insights into cost drivers and identify opportunities for optimization.

5.1 Economic Assumptions

The economic evaluation is based on a set of key assumptions outlined below.

- Capital costs and operating costs are obtained from Aspen Plus V12.1 Economic Analyzer tool.
- 2025 Chemical Engineering Plant Cost Index (CEPCI) value is estimated as 731.46 which is extrapolated from the previous year data [Manchester, 2023].
- Electricity price is taken as the most updated price, which is 69.96 EUR/MWh from May 2025 [Ember, 2024].
- Depreciation is not included in cost analysis.
- Investment period takes 3 years from 2025 until 2028 where the first year is spared for the feasibility study and 20 years of operation is considered during the calculations.
- Consumer Price Index (CPI) is taken as 1.5 % [Denmark, 2025].
- Discounting rate is taken as 3.5 %.
- Money exchange rate is taken as 1.08 \$/€.
- Economic feasibility is assessed using methods, Net Present Worth (NPV) and Levelized Cost of SAF (LCOSAF).

5.2 Economic Analysis Methodology

5.2.1 Equipment Costs

Capital and operating cost values are primarily obtained from the Aspen Plus V12.1 Economic Analyzer. However, for the reactors, except the methanol synthesis reactor (MeOH-R), equipment sizing is not performed in Aspen. Instead, capital costs for these reactors

are estimated externally using scaling methods. Table 5.1 summarizes the reference capital costs and scaling parameters used for the reactors in the MtJ process model. The capital cost of each reactor is calculated using the following scaling equation:

$$EC = \cdot EC_{\text{ref}} \cdot \left(\frac{S}{S_{\text{ref}}} \right)^{n} \tag{5.1}$$

where EC is the estimated equipment cost, EC_{ref} is the reference cost with a corresponding reference capacity $S_{\text{ref},i}$, a unit of size S, and a scaling exponent n, which allows cost estimation at other scales. The costs of these reactors are calculated with equation 5.1. The values used in the equation are listed in Table 5.1.

Table 5.1: Reactor costs and scaling parameters [Eyberg et al., 2024].

Equipment	$EC_{\textbf{ref}}$	$S_{\textbf{ref},i}$	S_{max}	**Unit of Size** S	n	**Year**
MTO reactor	0.1313 M€	3	–	t/h (feed)	0.72	2020
Oligomerization reactor	1.68 M€	320	–	mol/s (feed)	0.65	2011
Hydrogenation	0.694 M€	0.93	–	t/h (liquid feed)	0.70	2018

To reflect present-day economic conditions, equipment costs based on previous years data must be adjusted using the Chemical Engineering Plant Cost Index (CEPCI). For years when CEPCI data is not yet available (e.g., 2024 and 2025), extrapolated values are used based on historical trends. The CEPCI values used in this work are presented in Table 5.2, covering the period from 2000 to 2023. The values for 2024 and 2025 are obtained via extrapolation. The source for the CEPCI data is [Manchester, 2023].

Table 5.2: CEPCI values from 2000 to 2023 (2024 and 2025 extrapolated) [Manchester, 2023].

Year	**CEPCI**	**Year**	**CEPCI**
2000	394.1	2013	567.3
2001	394.3	2014	576.1
2002	395.6	2015	556.8
2003	402.0	2016	541.7
2004	444.2	2017	567.5
2005	468.2	2018	603.1
2006	499.6	2019	607.5
2007	525.4	2020	596.2
2008	575.4	2021	708.8
2009	521.9	2022	816.0
2010	550.8	2023	800.0
2011	585.7	2024	731.5
2012	584.6	2025	746.1

To update the original equipment cost to present values using CEPCI, Equation 5.2 is applied:

$$\text{Present Cost} = \text{Original Cost} \times \left(\frac{\text{Present Cost Index}}{\text{Original Cost Index}} \right) \tag{5.2}$$

5.2.2 Cash Flow Analysis

Cash flow represents the yearly net expenditure in the system and is used to evaluate the total cost of fuel production over the project lifetime. The general formulation of annual cash flow, including revenue, depreciation, and tax, is shown in Equation 5.3 [Peters et al., 2003]:

$$A_j = (s_j - co_j - d_j) \cdot (1 - \theta) + d_j \tag{5.3}$$

where A_j is annual cash flow in year j, $s_j$is sales revenue, co_j is cost of manufacturing which includes capital expenditures (CAPEX) and operating costs (OPEX), d_j is depreciation and θ is income tax rate.

In this study, depreciation and sales revenue are excluded to align with the LCOSAF framework. Since revenue is not included, income tax is also excluded because there is no taxable income without the inclusion of revenue. Instead, cash flows consist of CAPEX during the construction phase and annual OPEX during the production phase. Thus, the simplified expression becomes:

$$A_j = -\text{CAPEX}_j - \text{OPEX}_j \tag{5.4}$$

To account for inflation, both CAPEX and OPEX values are expressed in nominal (inflated) terms as they are escalated annually using a general consumer price inflation rate (CPI). The inflated cost in year j is calculated as:

$$C_j = C_0 \cdot (1 + f)^t \tag{5.5}$$

where C_j is the cost in year j which can be OPEX or CAPEX, adjusted for inflation, C_0 is base year cost (initial CAPEX or OPEX), f is annual inflation rate, and $t$is the number of years after the base year.

Consequently, the discount rate applied in the net present value (NPV) calculation is also nominal to maintain consistency with the inflated cash flows.

The net present value (NPV) represents the amount of money earned over and above the repayment of all investments and the earnings on the investments at the discount (or earning) rate used in the present worth factor (PWF) calculations. The NPV is defined by Equation (5.6):

$$\text{NPV} = \sum_{j=1}^{n} (A_j \times (1+i)^{-j}) \tag{5.6}$$

where A_j is cash flow, i is the discount rate. $(1+i)^{-j}$ overall is called present worth factor (PWF).

5.2.3 Levelized Cost of Sustainable Aviation Fuel Calculation

The LCOSAF is calculated by dividing the net present value (NPV) of total costs over the plant's lifetime by the total mass of SAF produced during the same period. This method accounts for the time value of money by discounting annual cash flows and aggregates the fuel output over the full operational horizon (see Appendix D).

$$\text{LCOSAF} = \frac{\text{NPV}}{\sum_{j=1}^{n} P_j} \tag{5.7}$$

where LCOSAF is in [€/tonne], NPV is the net present value of all costs over the plant lifetime [€], P_j is the amount of SAF produced in year j [tonne/year], n is the plant lifetime [years].

5.3 Economic Results

Figure 5.1 illustrates the capital cost distribution across different sections of the MtJ process for the year 2025. The methanol synthesis section (MEOH-SYN) includes the equipment: K-101, E-100, R-100 (MEOH-R), E-101, E-107, and E-108. The methanol-to-olefins (MTO) section consists of E-102, V-101, E-103, R-101 (MTO-R), K-104, R-102 (REGEN-R), E-104, and V-102. The oligomerization (OLI) unit comprises K-102, E-105, R-103 (OLI-R), and K-103. The hydrogenation (HYDRO) section includes E-106 and R-104 (HYDRO-R). Finally, the refining unit (REFIN) consists of V-103, V-104, and C-100 (KERCOL). (see Figures 4.1, 4.2)

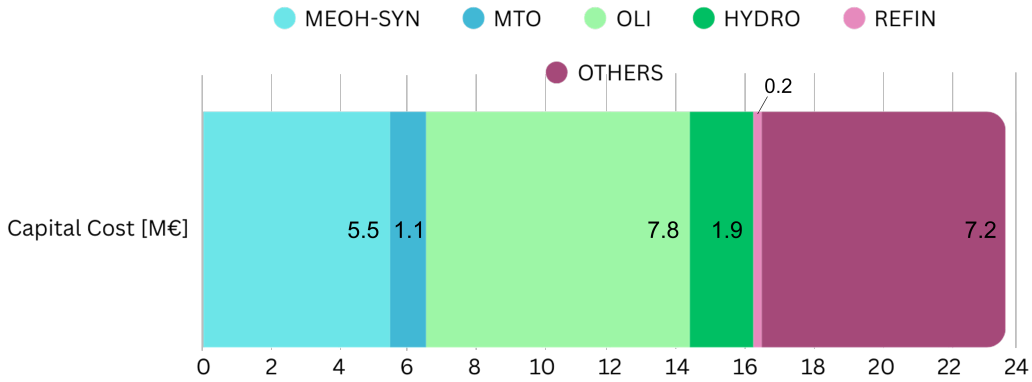

Figure 5.1: Capital breakdown of MtJ process.

The largest share of the investment is attributed to the oligomerization and methanol synthesis sections. This high share is likely due to the intensity of compressors and heat exchangers in those sections. Because of their high capital intensity, the OLI and MEOH-SYN sections might be particularly sensitive to design changes, which can significantly influence total investment. The remaining capital is distributed among the MTO, HYDRO, and REFIN sections. The "other costs" category captures indirect capital expenditures such as installation, contingency, engineering, and project management, which are not itemized by Aspen but significantly influence the total investment. The refining section accounts for only a minor fraction of the total capital cost. This is likely due to its relatively simple separation duties and the use of smaller or less complex equipment. Additionally, the low contribution may be partly attributed to the simplified modeling of the distillation column (KERCOL), which was represented as a RADFRAC block in Aspen. Overall. this breakdown highlights the relative cost impact of each processing step, guiding future optimization efforts and cost-reduction strategies.

Figure 5.2 presents the breakdown of raw material and utility costs in the MtJ process for 2025.

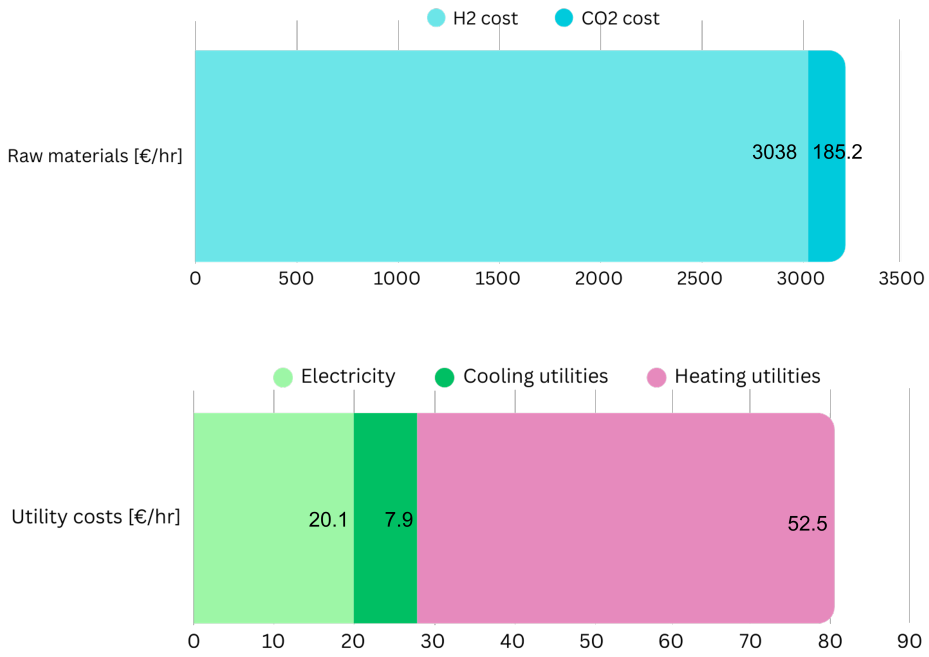

Figure 5.2: Raw material cost (top) and utility cost (bottom) breakdown across major units in the MtJ process (2025).

Raw materials account for the majority of operating costs, with hydrogen alone contributing over 94% of the raw material cost. At an assumed market price of 4 \$/kg (converted to 3.70 €/kg [Vickers et al., 2020]), hydrogen supply represents a key economic driver of the process. CO_2 contributes marginally to the total, at a cost of 0.025 \$/kg (0.023 €/kg [IEA, 2021]). Among utilities, heating utilities are the most significant, suggesting potential benefits from heat integration or process redesign. Electricity and cooling demands are comparatively lower. Overall, the results emphasize the need for hydrogen cost optimization and thermal efficiency improvements to enhance the economic viability of the MtJ pathway.

5.3.1 Levelized Cost of Sustainable Aviation Fuel Results

Figure 5.3 presents a comparison of the levelized cost of sustainable aviation fuel (LCOSAF) for this study's base and optimized cases against literature benchmarks from 2025.

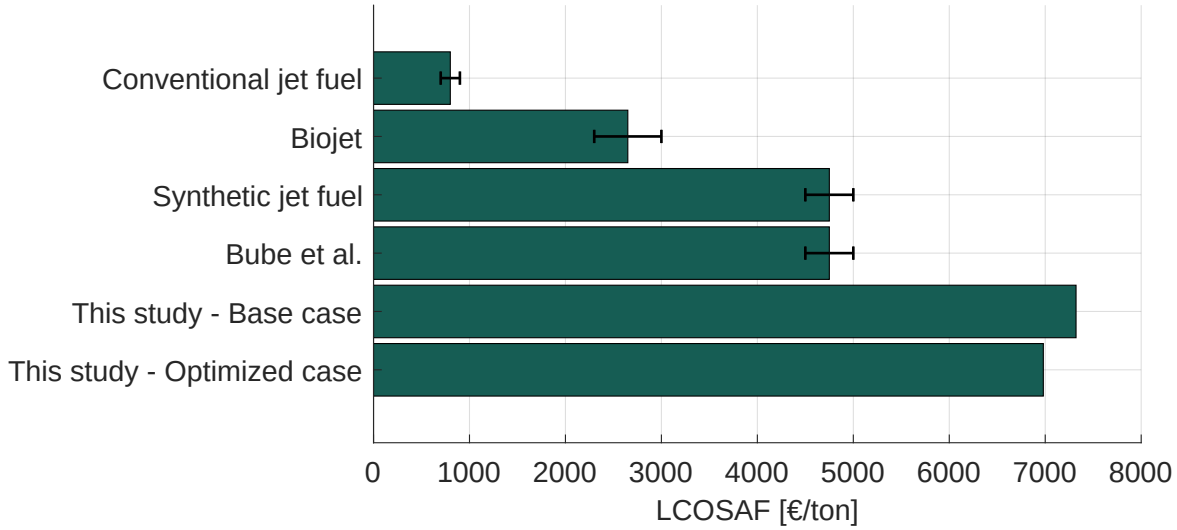

Figure 5.3: LCOSAF comparison with literature benchmarks. [Bube et al., 2025], [Bassanino et al., 2024]

The optimized MtJ configuration achieves an LCOSAF of 6980 €/tonne, slightly lower than the base case at 7321 €/tonne, indicating moderate economic improvements through process optimization. These values are compared with literature benchmarks, including estimates by Bube et al., which also analyze the MtJ pathway under similar assumptions (e.g., oligomerization selectivity of 90 %) and report LCOSAF in the range of 4500–5000 €/tonne [Bube et al., 2025]. Other synthetic fuel studies, report similar cost ranges as 4500–5000 €/tonne. Conventional fossil-derived jet fuel remains significantly cheaper (700–900 €/tonne), while biojet fuels are reported in the range of 2300–3000 €/tonne. [Bassanino et al., 2024]

The large cost gap between synthetic and conventional jet fuels highlights the prevailing economic barriers to e-fuel deployment. However, this price difference does not account for environmental externalities, such as lifecycle carbon emissions, which are increasingly being internalized through regulatory measures. As SAF becomes central to achieving aviation decarbonization targets—such as the EU's ReFuelEU initiative mandating a 2 % SAF blend by 2025 and reaching 70 % by 2050 [Larsen et al., 2023]. By comparing the synthetic and conventional fuel prices, the role of policy support seems critical to ensure competitiveness. Stable policies, revenue guarantee mechanisms, and incentives for low-carbon hydrogen and CO_2 are crucial to make synthetic fuels cost-competitive.

For this study specifically, further reductions in LCOSAF may be achievable through strategies such as heat integration, improved carbon and energy efficiencies, and access

to lower-cost hydrogen and CO_2 sources. Heat integration could reduce utility demand, particularly for heating, which accounts for a significant share of the utility cost. Additionally, as shown in sensitivity analyses by Bube et al., hydrogen and CO_2 feedstock prices are among the most influential factors in production cost variance [Bube et al., 2025]. This sensitivity is clearly reflected in the current study as well. As shown in Figure 5.2, raw material costs, particularly hydrogen, takes the dominant portion of operational expenditure. This highlights the strong dependency of the MtJ process on feedstock pricing and emphasizes the economic benefit of securing low-cost, renewable hydrogen and captured CO_2.

This significant cost gap also emphasizes the critical role of policy. According to Johnson Matthey, narrowing this gap will require a combination of long-term regulatory stability, carbon pricing, and dedicated SAF mandates to incentivize investment and de-risk production. Such regulations such as ReFuelEU Aviation not only provide market certainty but also help close the cost gap between fossil and synthetic fuels—especially as technological advancements and scale economies begin to take effect. [Johnson Matthey, 2024] In the long run, scaling up production and using a wider range of feedstocks which will increase supply-side flexibility can help bring SAF prices down. This market-driven cost reduction will be important for closing the price gap with fossil jet fuel and making it more affordable for airlines, supporting wider use of sustainable aviation fuels.

Chapter 6

Discussion

In this study, a comprehensive Aspen Plus process model was developed to design and evaluate a methanol-to-jet (MtJ) synthesis pathway for producing sustainable aviation fuel (e-SAF) from CO_2 and hydrogen. The flowsheet includes all major conversion steps: a methanol synthesis reactor primarily generating methanol, a methanol-to-olefins (MTO) reactor producing mainly light C_2–C_4 olefins, an oligomerization reactor converting these olefins into heavier hydrocarbons in the C_6–C_{24} range, and a hydrotreatment reactor for saturating the olefins to paraffins. To capture the effect of operating conditions on product distribution, a model was developed on MATLAB, and the Aspen Plus simulation was dynamically coupled with MATLAB and Excel, enabling real-time updates of the oligomerization product distribution in response to changes in inlet temperature and pressure.

Following the process modeling, an optimization strategy was implemented to simultaneously maximize kerosene yield and minimize capital cost by varying selected operating parameters: methanol reactor pressure, and both the temperature and pressure of the oligomerization reactor. A central composite design (CCD) was employed to systematically generate simulation data across the parameter space. The resulting data were then used to fit response surface models, which were then used during multi-objective optimization.

Multi-objective optimization generated a Pareto front which shows higher kerosene production required a higher expense of equipment costing due to more severe operating conditions for the oligomerization unit. Although milder conditions were selected and a compressor got removed for the methanol synthesis step, the overall cost did not decrease significantly, as lower pressure led to reduced conversion and thus increased recycling of unreacted gases. Within the Pareto front, a compromise "knee point" was identified that offered an optimal balance between performance and investment. The optimized configuration achieved a significantly higher kerosene fraction compared to the base case, highlighting the effectiveness of targeted process tuning. These results show that combining process simulation and optimization is useful for making methanol-to-jet fuel production more efficient and cost-effective.

From the techno-economic analysis, the levelized cost of e-SAF (LCOSAF) which is 6980 €/tonne remained well above current fossil-jet prices. For example, Bube et al. predicted MtJ-SAF costs of 4500–5000 €/tonne for 2025 which is roughly six times today's jet fuel price [Bube et al., 2025] [Bassanino et al., 2024]. Raw materials, especially renewable hydrogen, dominated operating costs, echoing other studies that find electricity and H^2 to be the largest cost drivers in PtL processes. Johnson Matthey likewise re-

ports that SAF currently costs 2–7 times conventional jet fuel [Johnson Matthey, 2024]. This persisting price gap implies that economic viability will depend on external factors, mostly to supportive policies to be competitive against their conventional counterparts. Carbon pricing and blending mandates (e.g. EU ReFuelEU requirements) are needed to close the fossil/e-SAF cost gap. EU regulations will soon mandate a minimum SAF blending target of 2 % in 2025 and reaching up to 70 % by 2050, which should drive demand and scale [Larsen et al., 2023]. In addition, further reductions in cost are anticipated as technological readiness level increases and production efficiencies improve over time [Bassanino et al., 2024]. It should also be noted that the economic assessment in this study focused solely on kerosene as the target product. A more comprehensive evaluation that includes potential revenues from by-products such as naphtha and diesel may reveal improved profitability and better reflect the full value of the MtJ process. This suggests that future studies should explore multi-product allocation strategies when assessing economic performance.

The MtJ simulation model has several strengths. It integrates all key process steps: CO_2 hydrogenation to methanol, methanol-to-olefins (MTO), olefin oligomerization, and hydrogenation. Unlike some prior work with fixed product distribution from the experimental data, this study's oligomerization section uses a pressure- and temperature-dependent distribution, enabling realistic optimization of kerosene range output.

Despite these strengths, the model also has limitations. Like all steady-state simulations, it omits dynamic behaviors: start-up effects, catalyst deactivation, transient operation. The used model for oligomerization reactor and fitted response surfaces (RSM) fitted to simulation points for optimization are highly accurate but still represent an approximation which may not capture all the mechanism. The techno-economic model also relies on several assumptions that will need refinement with pilot-scale data. Thus, while the integrated Aspen model with MATLAB integration approach is powerful, it must be validated against experiments and further tuned for large-scale realities.

On a broader level, the results highlight both the promise and the challenges of MtJ-based e-SAF production. One of the key advantages of the MtJ pathway lies in its modularity and flexibility. Unlike centralized Fischer–Tropsch (FT) systems that require integrated syngas production and extensive on-site infrastructure, MtJ can leverage e-methanol as a standardized, transportable feedstock [Liquid Wind, 2024]. While this study modeled the full pathway including green hydrogen production, CO_2 conversion, and methanol synthesis, the MtJ process can offer the flexibility to decouple these upstream steps from the final fuel production stages in practical applications. As a result, MtJ enables smaller, distributed units that can focus specifically on the conversion of e-methanol to synthetic crude, followed by refining and blending. This not only reduces system complexity and capital requirements but also allows for faster deployment, improved adaptability to

changing market conditions, and enhanced supply chain stability. Nevertheless, economic feasibility remains a significant challenge, with MtJ-based e-SAF still requiring policy support and technological innovation to become competitive with fossil-based alternatives.

In summary, the results confirm that the MtJ pathway is technically feasible and offers promising efficiency, but its commercial viability depends on the availability of low-cost renewable hydrogen, effective carbon pricing, efficient heat integration, increasing the carbon and hydrogen efficiency, potential by-product credits and mandated SAF blending targets.

Chapter 7

Conclusion & Future Work

7.1 Conclusion

The transition toward sustainable aviation fuel (SAF) is essential to decarbonize the aviation sector, and electro-based synthetic kerosene (e-SAF) produced via the methanol-to-jet (MtJ) pathway presents a promising route. This thesis presented the modeling and optimization of a methanol-to-jet (MtJ) process for sustainable aviation fuel (e-SAF) production from CO_2 and renewable hydrogen. A detailed Aspen Plus model was developed to simulate the full pathway including methanol synthesis, methanol-to-olefins (MTO), oligomerization, and hydrogenation, while MATLAB and Excel were integrated to enable dynamic product distribution updates and multi-objective optimization.

The base case scenario resulted in a kerosene yield of 0.2104, which was improved to 0.3945 through optimization, nearly doubling the product yield. Moreover, the annual production rate increased significantly from 2103 to 9395 tonnes, indicating a substantial improvement. This improvement was achieved by adjusting key operating parameters: methanol synthesis pressure and oligomerization temperature. The corresponding levelized cost of SAF (LCOSAF) decreased from 7321 €/tonne in the base case to 6980 €/tonne in the optimized scenario. While this represents moderate improvement, the LCOSAF still exceeds current market prices for fossil-based jet fuels.

The LCOSAF can be reduced with increasing the carbon and hydrogen efficiency, with an efficient heat integration and inclusion of byproducts. Other operating strategies can also be conducted, not only the operating conditions but also the process configurations. The findings also reinforce that while the MtJ route is technically feasible and relatively efficient in general, its economic viability depends heavily on raw material cost, and policy support.

The flexibility of using e-methanol as a transportable feedstock enables decentralized and modular production, reducing infrastructure requirements and enhancing adaptability. This modularity provides a strategic advantage in scaling up e-SAF production and adjusting to fluctuating supply and demand conditions. Nevertheless, closing the cost gap with fossil fuels will require a combination of supportive policies such as carbon pricing, SAF blending mandates, and financial incentives, as well as further technological improvements.

With continued innovation and supportive policy frameworks, the MtJ pathway has strong potential to become a key enabler in the transition to low-carbon aviation fuel

systems and to help meet long-term climate goals.

7.2 Future Work

There are several opportunities which can be future work to improve both technical accuracy and economic performance.

- **Heat Integration and Energy Efficiency:** Future investigations should focus on implementing heat integration across unit operations to reduce utility demands and overall operating costs. For example, recovering heat from the exothermic methanol and oligomerization reactions could offset energy use in the recycle heating of non-reacted gases in the methanol synthesis section and MTO reactor or product separation stages. A pinch analysis approach could be applied to evaluate the process-wide energy optimization potential.

- **Dynamic and Flexible Operation:** As with other electro-fuel systems, MtJ plants will likely be affected by variable renewable electricity supply. Dynamic modeling could be performed to evaluate part-load operation, start-up/shutdown behavior, and demand-side flexibility. This would enable assessment of profitability under fluctuating electricity prices and grid conditions, and support integration with power markets. Additionally, if electrolyzer modeling is included, the impact of fluctuating electricity load on hydrogen production and overall process performance could also be analyzed.

- **By-product Strategies** This study focused only on kerosene as the target product. Future work should incorporate the economic contribution of by-products such as naphtha, diesel-range hydrocarbons, and light ends. Incorporating multi-product allocation strategies can improve revenue streams, and it should also be investigated whether integrating additional refining units for by-product upgrading or recycling them back into the process is technically and economically feasible.

- **Life-Cycle and Environmental Assessment:** A lifecycle assessment (LCA) of the MtJ process—including CO_2 capture, hydrogen production, methanol synthesis, and refining can help measure the total emissions saved. Comparing the carbon footprint of MtJ e-SAF to fossil jet fuel would provide stronger support for its environmental benefits.

- **Techno-Economic Sensitivity and Policy Scenarios** Conducting a sensitivity analysis on key economic parameters, such as electricity cost, hydrogen price, and SAF selling price, can help identify cost drivers and break-even points. Additionally, simulating policy scenarios (carbon pricing, subsidies, SAF mandates, etc.) can support strategic planning for commercial deployment.

Bibliography

[Aguayo et al., 2010] Aguayo, A. T., Mier, D., Gayubo, A. G., Gamero, M., and Bilbao, J. (2010). Kinetics of methanol transformation into hydrocarbons on a hzsm-5 zeolite catalyst at high temperature (400550 °c). *Industrial & Engineering Chemistry Research*, 49(24):12371–12378.

[Al Wahabi and Froment, 2004] Al Wahabi, S. M. and Froment, G. F. (2004). Single event kinetic modeling of the methanol-to-olefins process on sapo-34. *Industrial & Engineering Chemistry Research*, 43(17):5098–5111.

[Al Wahabi, 2003] Al Wahabi, S. M. H. (2003). *Conversion of Methanol to Light Olefins on SAPO-34*. PhD thesis, Texas A&M University.

[Alberty, 1987] Alberty, R. A. (1987). Kinetics of the polymerization of alkenes on zeolites. *The Journal of Chemical Physics*, 87(6):3660–3667.

[Arora, 2016] Arora, J. S. (2016). *Introduction to Optimum Design*. Academic Press, Oxford, UK, 4 edition.

[Aspen Technology, Inc., 2021] Aspen Technology, Inc. (2021). *Aspen Plus Methanol Synthesis Model*. Aspen Technology, Inc., Bedford, MA, USA. Proprietary and confidential document.

[ASTM International, 2012] ASTM International (2012). Standard specification for aviation turbine fuel containing synthesized hydrocarbons. `https://www.astm.org/D7566-12a.html`. Designation: D7566-12a. Approved November 1, 2012. Published February 2013.

[Avidan, 1988] Avidan, A. (1988). Gasoline and distillate fuels from methanol. In Bibby, D., Chang, C., Howe, R., and Yurchak, S., editors, *Methane Conversion*, volume 36 of *Studies in Surface Science and Catalysis*, pages 307–323. Elsevier.

[Bassanino et al., 2024] Bassanino, A., Calvi-Parisetti, F., and Sachdeva, N. (2024). Reaching refueleu: Development of the sustainable aviation fuels market at scale. `https://www.rolandberger.com/en/Insights/Publications/Reaching-ReFuelEU-development-of-the-sustainable-aviation-fuels-market-at-scale.html`. Accessed: 2025-05-24.

[Börner, 2014] Börner, L. (2014). *Methanol-based Hydrocarbon Synthesis: Kinetics and Reaction Engineering Aspects*. Springer, Berlin, Heidelberg.

[Bube et al., 2024] Bube, S., Bullerdiek, N., Voß, S., and Kaltschmitt, M. (2024). Kerosene production from power-based syngas – a technical comparison of the fischer-tropsch and methanol pathway. *Fuel*, 366:131269.

[Bube et al., 2025] Bube, S., Voß, S., Quante, G., and Kaltschmitt, M. (2025). Cost analysis of kerosene production from power-based syngas via the fischer-tropsch and methanol pathway. *Fuel*, 384:133901.

[Bussche and Froment, 1996] Bussche, K. M. V. and Froment, G. B. (1996). A steady-state kinetic model for methanol synthesis and the water gas shift reaction on a commercial copper-based catalyst. *Journal of Catalysis*, 161(1):1–10.

[Chang et al., 2013] Chang, J., Zhang, K., Chen, H., Yang, Y., and Zhang, L. (2013). Cfd modelling of the hydrodynamics and kinetic reactions in a fluidised-bed mto reactor. *Chemical Engineering Research and Design*, 91(12):2355–2368.

[Chen et al., 2007] Chen, D., Grønvold, A., Moljord, K., and Holmen, A. (2007). Methanol conversion to light olefins over sapo-34: Reaction network and deactivation kinetics. *Industrial & Engineering Chemistry Research*, 46(12):4116–4123.

[Chirita, 2024] Chirita, I. (2024). Long-term outlook for e-fuels in europe. `https://www.wko.at/oe/oegew/long-term-outlook-for-e-fuels-in-europe.pdf`.

[CIP, 2025] CIP (2025). Fjordptx. Last seen: 1/11-2024, `www.fjord-ptx.com`.

[Clarkfeldt and Kristensen, 2024] Clarkfeldt, A. T. and Kristensen, A. F. (2024). Assessment of utilisation and production of e-saf through mtj-synthesis to cover the fuel demand at cph airport in 2050.

[Cordero-Lanzac et al., 2024] Cordero-Lanzac, T., Gayubo, A. G., Aguayo, A. T., and Bilbao, J. (2024). The mto and dto processes as greener alternatives to produce olefins: A review of kinetic models and reactor design. *Chemical Engineering Journal*, 494:152906.

[Denmark, 2025] Denmark, S. (2025). Denmark - consumer price index. `https://www.dst.dk/en/Statistik/emner/oekonomi/prisindeks/forbrugerprisindeks#:~:text=The%20consumer%20price%20index%20follows,is%20a%20key%20economic%20figure.`. Accessed: 2025-05-01.

[Dubray et al., 2022] Dubray, F., Paunović, V., Ranocchiari, M., and van Bokhoven, J. A. (2022). Production of jet-fuel-range olefins via catalytic conversion of pentene and hexene over mesoporous al-sba-15 catalyst. *Journal of Industrial and Engineering Chemistry*, 114:409–417.

[Ember, 2024] Ember (2024). European wholesale electricity price data. `https://ember-energy.org/data/european-wholesale-electricity-price-data/`. Accessed: 2024-05-22.

[Energy, 2025] Energy, E. (2025). European energy – power-to-x solutions. Last seen: 05/04-2025, `www.fjord-ptx.com`.

[Eyberg et al., 2024] Eyberg, V., Dieterich, V., Bastek, S., Dossow, M., Spliethoff, H., and Fendt, S. (2024). Techno-economic assessment and comparison of fischer–tropsch and methanol-to-jet processes to produce sustainable aviation fuel via power-to-liquid. *Energy Conversion and Management*, 315:118728.

[Fontalvo, 2014] Fontalvo, J. (2014). Using user models in MatlabÂ®within the Aspen PlusÂ®interface with an ExcelÂ®link. *IngenierÃa e InvestigaciÃ*, 34:39 – 43.

[Garwood, 1983] Garwood, W. E. (1983). *Conversion of C₂-C₁₀ to Higher Olefins over Synthetic Zeolite ZSM-5*, chapter 23, pages 383–396.

[IEA, 2021] IEA (2021). Is carbon capture too expensive? `https://www.iea.org/commentaries/is-carbon-capture-too-expensive`. Accessed: 2025-04-06.

[IEA Bioenergy Task 39, 2023] IEA Bioenergy Task 39 (2023). Progress in commercialization of biojet/sustainable aviation fuels. Technical report, IEA Bioenergy.

[International Energy Agency, 2025] International Energy Agency (2025). Aviation – topics. Accessed: 2024-5-02-27.

[Johnson Matthey, 2024] Johnson Matthey (2024). The price of sustainable aviation fuel. `https://matthey.com/media/expert-insights/the-price-of-sustainable-aviation-fuel`. Accessed: 2025-05-24.

[Kaarsholm et al., 2010] Kaarsholm, M., Rafii, B., Joensen, F., Cenni, R., Chaouki, J., and Patience, G. S. (2010). Kinetic modeling of methanol-to-olefin reaction over zsm-5 in fluid bed. *Industrial & Engineering Chemistry Research*, 49(1):29–38.

[Kaltschmitt and Neuling, 2018] Kaltschmitt, M. and Neuling, U., editors (2018). *Biokerosene: Status and Prospects*. Springer, Berlin, Germany.

[Larsen et al., 2023] Larsen, M. N., Obeid, A., Münster, M., and Mathiesen, B. V. (2023). Renewable aviation e-saf: Catalogue and system impacts. `https://vbn.aau.dk/en/publications/renewable-aviation-e-saf-catalogue-and-system-impacts`. Accessed: April 2025.

[Liquid Wind, 2024] Liquid Wind (2024). Aviation — the role of emethanol in sustainable aviation fuel. `https://www.liquidwind.com/aviation`. Accessed: 2025-05-25.

[Maitlis and de Klerk, 2013] Maitlis, P. and de Klerk, A. (2013). *Greener Fischer-Tropsch Processes: For Fuels and Feedstocks*. Wiley. ISBN: 9783527329458.

[Manchester, 2023] Manchester, U. (2023). Cepci: Chemical engineering plant cost index. `https://www.training.itservices.manchester.ac.uk/public/gced/CEPCI.html?reactors/CEPCI/index.html`. Accessed: 8-12-2024.

[Mignard and Pritchard, 2008] Mignard, D. and Pritchard, C. (2008). On the use of electrolytic hydrogen from variable renewable energies for the enhanced conversion of biomass to fuels. *Chemical Engineering Research and Design*, 86(5):473–487.

[Minitab, 2025] Minitab (2025). Response surface designs: Central composite and box-behnken designs. https://support.minitab.com/en-us/minitab/help-and-how-to/statistical-modeling/doe/supporting-topics/response-surface-designs/response-surface-central-composite-and-box-behnken-designs/. Accessed: 2025-05-21.

[Montgomery, 2017] Montgomery, D. C. (2017). *Design and Analysis of Experiments*. John Wiley & Sons, 9th edition.

[Nicholas, 2017] Nicholas, C. P. (2017). Applications of light olefin oligomerization to the production of fuels and chemicals. *Applied Catalysis A: General*, 543:82–97.

[NIST/SEMATECH, 2012] NIST/SEMATECH (2012). Nist/sematech e-handbook of statistical methods, section 3.3.6.1: Polynomial regression models. https://www.itl.nist.gov/div898/handbook/pri/section3/pri3361.htm. Accessed: 2025-05-21.

[Ortiz-Espinoza et al., 2017] Ortiz-Espinoza, A. P., Noureldin, M. M., El-Halwagi, M. M., and Jiménez-Gutiérrez, A. (2017). Design, simulation and techno-economic analysis of two processes for the conversion of shale gas to ethylene. *Computers Chemical Engineering*, 107:237–246. In honor of Professor Rafiqul Gani.

[Peters et al., 2003] Peters, M., Timmerhaus, K., and West, R. (2003). *Plant Design and Economics for Chemical Engineers*. McGraw-Hill chemical engineering series. McGraw-Hill Education. ISBN: 9780072392661.

[Rumizen, 2021] Rumizen, M. A. (2021). Qualification of alternative jet fuels. *Frontiers in Energy Research*, 9. https://www.frontiersin.org/journals/energy-research/articles/10.3389/fenrg.2021.760713.

[Ruokonen et al., 2021] Ruokonen, J., Nieminen, H., Dahiru, A. R., Laari, A., Koiranen, T., Laaksonen, P., Vuokila, A., and Huuhtanen, M. (2021). Modelling and cost estimation for conversion of green methanol to renewable liquid transport fuels via olefin oligomerisation. *Processes*, 9(6).

[Salkuyeh and Adams, 2015] Salkuyeh, Y. K. and Adams, T. A. (2015). Co-production of olefins, fuels, and electricity from conventional pipeline gas and shale gas with near-zero co2 emissions. part i: Process development and technical performance. *Energies*, 8(5):3739–3761.

[Schmidt and Weindorf, 2018] Schmidt, P. R. and Weindorf, W. (2018). Power-to-liquids as renewable fuel option for aviation: A review. *Energy Technology*, 6(5):1048–1057.

[Shell, 2024] Shell, A. D. (2024). Jeta1; msds no. 800001002769. https://www.epc.shell.com/DocumentManagement/DocumentRequest/108238407?Name=Jet%20A-1&Type=MSDS.

[Tabak et al., 1986] Tabak, S. A., Krambeck, F. J., and Garwood, W. E. (1986). Conversion of propylene and butylene over zsm-5 catalyst. *AIChE Journal*, 32(9):1526–1531.

[Tahan, 2022] Tahan, M.-R. (2022). Recent advances in hydrogen compressors for use in large-scale renewable energy integration. *International Journal of Hydrogen Energy*, 47(83):35275–35292.

[Taheri Najafabadi et al., 2012] Taheri Najafabadi, A., Fatemi, S., Sohrabi, M., and Salmasi, M. (2012). Kinetic modeling and optimization of the operating condition of mto process on sapo-34 catalyst. *Journal of Industrial and Engineering Chemistry*, 18(1):29–37.

[UNFCCC, 2018] UNFCCC (2018). Submission to the unfccc on behalf of the international civil aviation organization (icao). `https://www4.unfccc.int/sites/SubmissionsStaging/Documents/201804271412---SBSTA48%20ICAO%20submission_final.pdf`. Accessed: April 2025.

[Vandal and Bouallou, 2013] Vandal, S. and Bouallou, C. (2013). Design and simulation of a methanol production plant from co2 hydrogenation. *Journal of Cleaner Production*, 57:38–45.

[Vickers et al., 2020] Vickers, J., Peterson, D., and Randolph, K. (2020). Cost of electrolytic hydrogen production with existing technology. `https://www.hydrogen.energy.gov/docs/hydrogenprogramlibraries/pdfs/20004-cost-electrolytic-hydrogen-production.pdf?Status=Master`. Accessed: 2025-04-06.

[Vora et al., 1997] Vora, B., Marker, T., Barger, P., Nilsen, H., Kvisle, S., and Fuglerud, T. (1997). Economic route for natural gas conversion to ethylene and propylene. In de Pontes, M., Espinoza, R., Nicolaides, C., Scholtz, J., and Scurrell, M., editors, *Natural Gas Conversion IV*, volume 107 of *Studies in Surface Science and Catalysis*, pages 87–98. Elsevier.

[Wilson and Barger, 1999] Wilson, S. and Barger, P. (1999). The characteristics of sapo-34 which influence the conversion of methanol to light olefins. *Microporous and Mesoporous Materials*, 29(1):117–126.

[Ying et al., 2015] Ying, L., Yuan, X., Ye, M., Cheng, Y., Li, X., and Liu, Z. (2015). A seven lumped kinetic model for industrial catalyst in dmto process. *Chemical Engineering Research and Design*, 100:179–191.

[Yu and Chien, 2016] Yu, B.-Y. and Chien, I.-L. (2016). Design and optimization of the methanol-to-olefin process. part i: Steady-state design and optimization. *Chemical Engineering & Technology*, 39(12):2293–2303.

Appendix A

Component specifications

Table A.1: Component list used in the simulation.

Component ID	Type	Component Name	Alias
N2	Conventional	NITROGEN	N2
AR	Conventional	ARGON	AR
O2	Conventional	OXYGEN	O2
H2	Conventional	HYDROGEN	H2
CO	Conventional	CARBON-MONOXIDE	CO
CO2	Conventional	CARBON-DIOXIDE	CO2
NH3	Conventional	AMMONIA	H3N
H2O	Conventional	WATER	H2O
MEOH	Conventional	METHANOL	CH4O
ETOH	Conventional	ETHANOL	C2H6O-2
DME	Conventional	DIMETHYL-ETHER	C2H6O-1
CH4	Conventional	METHANE	CH4
C2H6	Conventional	ETHANE	C2H6
C3H8	Conventional	PROPANE	C3H8
N-C4	Conventional	N-BUTANE	C4H10-1
N-C5	Conventional	N-PENTANE	C5H12-1
N-C6	Conventional	N-HEXANE	C6H14-1
N-C7	Conventional	N-HEPTANE	C7H16-1
N-C8	Conventional	N-OCTANE	C8H18-1
N-C9	Conventional	N-NONANE	C9H20-1
N-C10	Conventional	N-DECANE	C10H22-1
N-C11	Conventional	N-UNDECANE	C11H24
N-C12	Conventional	N-DODECANE	C12H26
N-C13	Conventional	N-TRIDECANE	C13H28
N-C14	Conventional	N-TETRADECANE	C14H30
N-C15	Conventional	N-PENTADECANE	C15H32
N-C16	Conventional	N-HEXADECANE	C16H34
N-C17	Conventional	N-HEPTADECANE	C17H36
N-C18	Conventional	N-OCTADECANE	C18H38
N-C19	Conventional	N-NONADECANE	C19H40
N-C20	Conventional	N-EICOSANE	C20H42
N-C21	Conventional	N-HENEICOSANE	C21H44
N-C22	Conventional	N-DOCOSANE	C22H46
N-C23	Conventional	N-TRICOSANE	C23H48
N-C24	Conventional	N-TETRACOSANE	C24H50
C2H4	Conventional	ETHYLENE	C2H4

Component ID	Type	Component Name	Alias
C3H6	Conventional	PROPYLENE	C3H6-2
1-C4H8	Conventional	1-BUTENE	C4H8-1
1-C5H10	Conventional	1-PENTENE	C5H10-2
1-C6H12	Conventional	1-HEXENE	C6H12-3
1-C7H14	Conventional	1-HEPTENE	C7H14-7
1-C8H16	Conventional	1-OCTENE	C8H16-16
1-C9H18	Conventional	1-NONENE	C9H18-3
1-C10H20	Conventional	1-DECENE	C10H20-5
1-C11H22	Conventional	1-UNDECENE	C11H22-2
1-C12H24	Conventional	1-DODECENE	C12H24-2
1-C13H26	Conventional	1-TRIDECENE	C13H26-2
1-C14H28	Conventional	1-TETRADECENE	C14H28-2
1-C15H30	Conventional	1-PENTADECENE	C15H30-2
1-C16H32	Conventional	1-HEXADECENE	C16H32-2
1-C17H34	Conventional	1-HEPTADECENE	C17H34-D1
1-C18H36	Conventional	1-OCTADECENE	C18H36-1
1-C19H38	Conventional	1-NONADECENE	C19H38-D1
1-C20H40	Conventional	1-EICOSENE	C20H40-D1
1-C21H42	Conventional	1-HENEICOSENE	C21H42-N2
1-C22H44	Conventional	1-DOCOSENE	C22H44-D1
1-C23H46	Conventional	1-TRICOSENE	C23H46-N3
1-C24H48	Conventional	1-TETRACOSENE	C24H48-D1
COKE	Conventional	CARBON-GRAPHITE	C

Appendix B

Reaction Model Validations

For each reactor model which includes a kinetic model, validation is applied before employing the reactors into the process system.

B.1 Methanol Synthesis Reactor Validation

The Aspen model, with the kinetic model given in Chapter 3, was validated with the data reported by Bussche et al. [Bussche and Froment, 1996]. A plug flow reactor (RPLUG) was used under isobaric and adiabatic conditions with a feed consisting of 4% CO, 82% H_2, 3% CO_2, and 11% inerts (Ar). The reactor used in the simulation was 0.15 m in length and 0.016 m in diameter, and it contained 34.8 g of catalyst with a density of 1775 kg/m^3 and a void fraction of 33%.

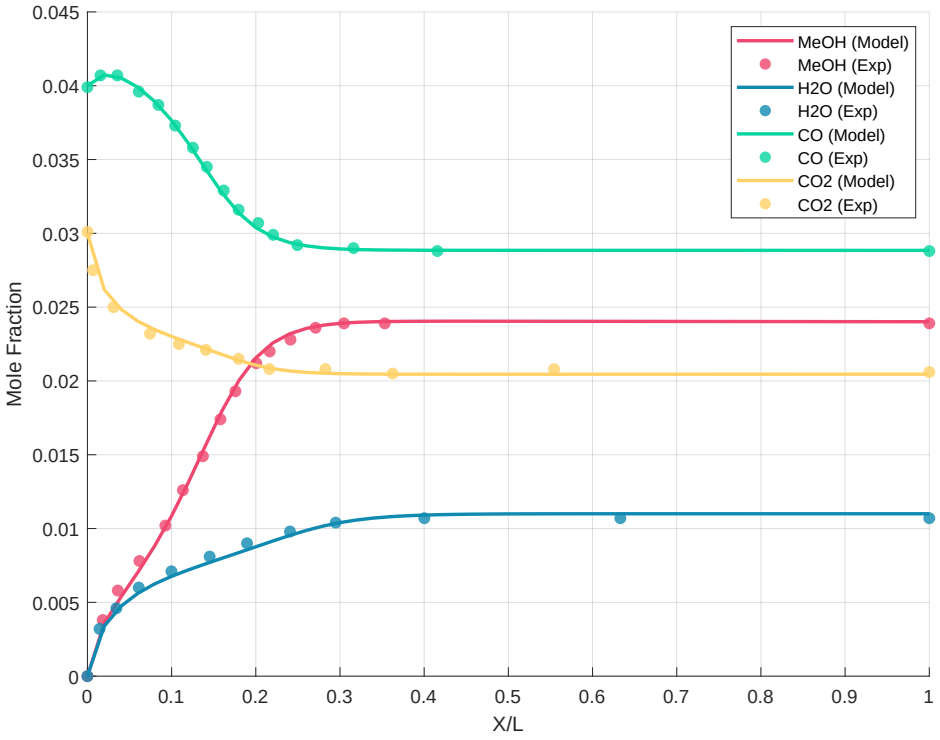

Figure B.1: Mole Fractions of the Aspen model vs. the experimental data at 50 bar and 220 °C.

Figure B.1 shows mole fraction profiles of MeOH, H_2O, CO, CO_2 along the reactor length which is normalized. The model and experimental data closely match. MeOH and H_2O formation and CO, CO_2 consumption trend captured well by the simulation, confirming that the model accurately reflects the reaction behavior along the reactor.

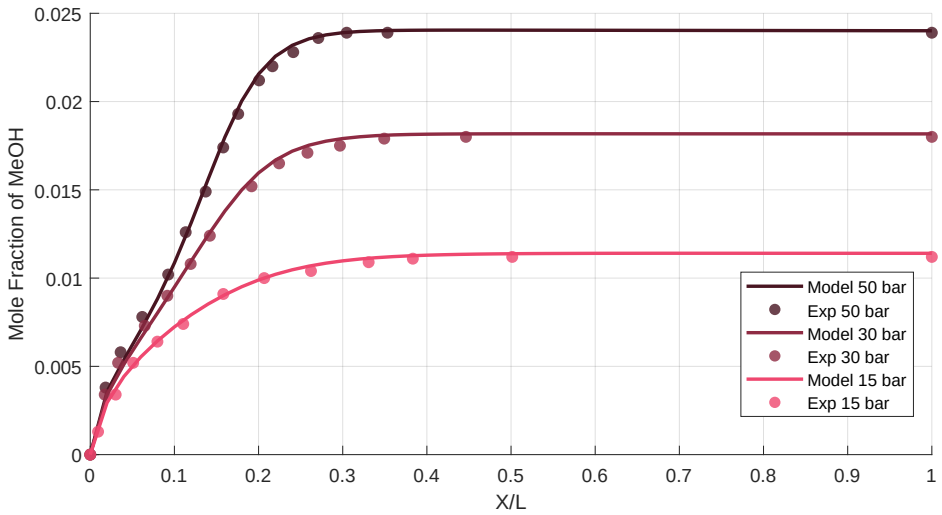

Figure B.2: Methanol mole fractions of the Aspen model vs. the experimental data with varying pressure at 220 °C.

Figure B.2 illustrates the effect of pressure on methanol formation at 15, 30, and 50 bar. As shown in the figure, the methanol mole fraction increases with rising pressure, indicating enhanced methanol production. This trend is consistent with Le Chatelier's principle, since the methanol synthesis reaction involves a net decrease in the number of gas-phase moles, hence an increase in pressure shifts the reaction to the product side (3.1). The model accurately captures this behavior across different pressures and shows good agreement with the experimental data.

Figures B.1 and B.2 demonstrate the strong agreement between the Aspen Plus simulation results and the experimental data. These results confirm that the Aspen Plus model, which is based on the Vanden Bussche and Froment kinetics, reliably captures the behavior of methanol synthesis. Therefore, it is suitable for use in process design and optimization.

Appendix C

Oligomerization Reactor Conversion Model

The conversion of light olefins to heavier products was modeled as a second-order function of temperature and pressure. The fitted model is given by:

$$X(T, P) = 0.0035 \cdot T - 1.8851 + 0.1210 \cdot P - 0.0035 \cdot P^2 \tag{C.1}$$

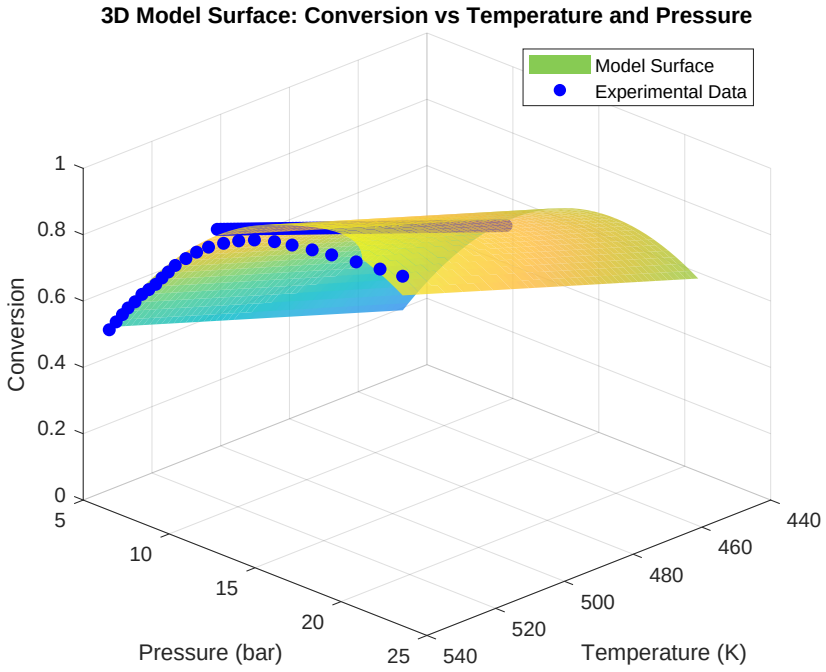

Figure C.1: 3D Model of Conversion vs Temperature and Pressure.

To ensure physically meaningful values, the conversion is bounded between 0 and 1. The model was fitted using nonlinear least squares regression and evaluated against experimental data. The performance metrics are: $R^2 = 0.9809$, RMSE = 0.0189, and MAE = 0.0149, indicating a good correlation between model predictions and the data.

Appendix D

Economic Evaluation Calculations

Table D.1: Annual Cash Flow Analysis for MtJ Plant.

Year ending at time	2025	2026	2027	2028	2029	2030	2031	2032
Year Index	-3	-2	-1	0	1	2	3	4
Total Capital, 106€		-3.55	-8.41	-12.19				
Operating capacity					0.5	0.9	1	1
Total OPEX,106€					-20.33	-37.15	-41.89	-42.52
Total annual cash flow, 106€	0	-3.55	-8.41	-12.19	-20.33	-37.15	-41.89	-42.52
Present worth factor	1.18	1.11	1.06	1.00	0.95	0.90	0.85	0.81
Present worth of annual cash flows, 106€	0	-3.96	-8.88	-12.19	-19.26	-33.33	-35.61	-34.23
23. Net present worth, 106€	-546.05							
SAF production per year, kg/year					2016.18	3629.12	4032.36	4032.36
Year ending at time	2033	2034	2035	2036	2037	2038	2039	2040
Year Index	5	6	7	8	9	10	11	12
Total Capital, 106€								
Operating capacity	1	1	1	1	1	1	1	1
Total OPEX,106€	-43.16	-43.81	-44.46	-45.13	-45.81	-46.49	-47.19	-47.90
Total annual cash flow, 106€	-43.16	-43.81	-44.46	-45.13	-45.81	-46.49	-47.19	-47.90
Present worth factor	0.76	0.72	0.68	0.65	0.61	0.58	0.55	0.52
Present worth of annual cash flows, 106€	-32.91	-31.64	-30.42	-29.25	-28.12	-27.04	-26.00	-24.99
23. Net present worth, 106€								
SAF production per year, kg/year	4032.36	4032.36	4032.36	4032.36	4032.36	4032.36	4032.36	4032.36
Year ending at time	2041	2042	2043	2044	2045	2046	2047	2048
Year Index	13	14	15	16	17	18	19	20
Total Capital, 106€								
Operating capacity	1	1	1	1	1	1	1	1
Total OPEX,106€	-48.62	-49.35	-50.09	-50.84	-51.60	-52.38	-53.16	-53.96
Total annual cash flow, 106€	-48.62	-49.35	-50.09	-50.84	-51.60	-52.38	-53.16	-53.96
Present worth factor	0.49	0.47	0.44	0.42	0.40	0.38	0.36	0.34
Present worth of annual cash flows, 106€	-24.03	-23.10	-22.21	-21.36	-20.53	-19.74	-18.98	-18.25
23. Net present worth, 106€								
SAF production per year, kg/year	4032.36	4032.36	4032.36	4032.36	4032.36	4032.36	4032.36	4032.36
Total SAF production over lifetime, tonnes over the plant lifetime	78227.79							
Levelized Cost of SAF, €/tonne	**6980.3**							